

Fleet and Vertiport Sizing for an Urban Air Mobility Commuting Service

Transportation Research Record
2024, Vol. 2678(8) 443–469
© The Author(s) 2024
Article reuse guidelines:
sagepub.com/journals-permissions
DOI: 10.1177/03611981231216977
journals.sagepub.com/home/trr



Mark T. Kotwicz Herniczek¹ , Brian J. German¹ , and Lukas Preis² 

Abstract

An understanding of fleet size and vertiport size sensitivity to demand and operational parameters is necessary to quantify the scalability of urban air mobility (UAM) services. In this work, we implement a bilevel rolling window fleet scheduling formulation that includes vertiport area as a secondary objective. We also present a simple vertiport area estimation methodology that leverages the fleet scheduling results and provides a lower bound on vertiport infrastructure area requirements. Lastly, we explore the sensitivity of fleet size and vertiport infrastructure requirements to several vehicle and operational parameters, including geographical demand distribution, daily passenger volume, vehicle passenger capacity, passenger aggregation window, battery charge rate, pad separation, and pad size. We find that, although the fleet size is reasonable for a UAM commuting service scaled to serve 10,000 passengers per day, vertiport area requirements are likely problematic under current sizing guidance from the Federal Aviation Administration, particularly area requirements for vertiports that serve as workplace hubs located in dense urban centers.

Keywords

aviation, urban air mobility

Urban air mobility (UAM) vertiport sizing and design are relatively new but fast-developing fields of research as it becomes clear that land infrastructure availability will likely limit the scalability of UAM operations (1–8). Although the application to electric vertical take-off and landing (eVTOL) vehicles is recent, vertiport design dates back to the 1960s, when helicopters were thought to be on the verge of providing an intracity transportation service comparable with UAM (2). Unsurprisingly, a majority of vertiport sizing and design research, including recent efforts by the Federal Aviation Administration (FAA) and European Aviation Safety Agency (EASA), are based on heliport guidelines because of the similarities between helicopters and eVTOL vehicles (9, 10).

In particular, vertiport topology design can significantly affect the efficiency and safety of UAM operations, and therefore has been a focus for researchers. Likewise, accurate estimation of vertiport throughput and capacity and an understanding of the sensitivity of these metrics to operational parameters are necessary to assess the scalability of UAM operations and have been explored by several authors. Notably, Vascik and Hansman developed an integer programming approach

to estimate vertiport capacity and determine the sensitivity of vertiport capacity to vertiport topology parameters, such as number of gates and pads, and to operational parameters, such as vehicle turnaround time and taxi time (5). Zelinski presented several generic vertiport topology designs and evaluated their relative surface area utilization and operational efficiency (11). Taylor et al. used a stochastic Monte Carlo simulation to calculate vehicle throughput for several vertiport configurations (12). Guerreiro et al. implemented a first-come, first-served vertiport scheduling algorithm to assess and compare the capacity and throughput of various vertiport configurations (13). Preis introduced four vertiport topologies and utilized a mixed integer programming approach to find the topology and number of pads and gates that maximize vertiport throughput (14). Lastly,

¹School of Aerospace Engineering, Georgia Institute of Technology, GA

²School of Engineering and Design, Technical University of Munich, Bavaria, Germany

Corresponding Author:

Mark T. Kotwicz Herniczek, mark.kotwicz@gatech.edu

Rimjha and Trani estimated the hourly vertiport capacity for three basic vertiport configurations using a discrete event simulation model and simulated UAM vertiport operations in the San Francisco business district area to estimate the serving capacity of vertiports (6).

Several authors have also focused on comparison of traffic management policies, vertiport requirements, and estimation of vertiport operational parameters. Goodrich and Barmore conducted a preliminary assessment of vertiport requirements relative to the feasibility of large-scale UAM operations (15). Li et al. used a simulation-based approach to analyze the impact of infrastructure, fleet constraints, and traffic management policies on UAM operational efficiency (16). Schweiger et al. conceptualized infrastructure parameters for generic vertiport operations, including pad topology, approach and departure mission profiles, and a generic set of operational rules for arrivals and departures (17). Finally, Preis and Hornung used an agent-based modeling and simulation framework to explore vertiport efficiency and conducted expert interviews to refine parameters relevant to vertiport operations, such as boarding, hover, and taxiing time (7).

The vertiport sizing in this work deviates from the literature in three notable ways. First, we extend a vehicle scheduling formulation to include vertiport sizing as a secondary objective to improve the quality of the scheduling solution used by the vertiport sizing model. Second, our sizing formulation attempts to form a lower bound on vertiport size rather than an accurate sizing estimate. As a result, pad configuration is less relevant, and the equations used to estimate vertiport size are significantly simpler and better demonstrate the influence of parameters on vertiport size. Lastly, the sensitivity of sizing estimates to a wide range of operational and vehicle parameters are presented. The motivation for developing a simple baseline model rather than using sizing estimates from the literature is twofold: first, available sizing estimates tend to have a complexity and input data requirements outside the scope of this work, and second, sizing estimates vary significantly within the literature (from 5.9 to 72 m² to accommodate a throughput of one passenger per hour) because of variations in vertiport design, vehicle choice, and operational parameters (5, 12, 14, 18, 19).

It should be noted that the paper focuses on commuting operations rather than other potential UAM services, such as airport-to-downtown, airport-to-airport, or longer-range regional air transportation services, even though an airport-airport shuttle service may be more viable in the near term because of their more uniform bi-directional flow of demand throughout the day, their higher concentration of demand, and their ability to capitalize on demand from business travelers. A focus is

placed on commuting operations for several reasons, namely 1) UAM has been heavily marketed as an alternative mode of transportation for commuting operations and 2) nationwide commuter flow and economic data are publicly available, facilitating nationwide demand studies and enabling comparison of regional results based on consistent data sources (3, 20–22). Although fleet and vertiport sizing are applied to commuter flow data, the presented models can be generalized to other sources of data to analyze the feasibility and scalability of other UAM services.

The structure of the paper is as follows. We first provide an overview of the vertiport sizing methodology, including how the sizing model leverages census commuting data and vertiport locations to obtain a passenger demand schedule. We then present a bilevel scheduling formulation that minimizes fleet repositioning flights, fleet size, and vertiport infrastructure requirements. A detailed description of the vertiport area estimation formulation is then provided. Next, we provide vertiport sizing results for Atlanta, San Francisco, New York City, and Seattle, U.S., based on a normalized commuting demand of 10,000 passengers per day. We then present sensitivity studies that explore the sensitivity of fleet size and vertiport infrastructure requirements to several vehicle and operational parameters, including daily passenger volume, vehicle passenger capacity, passenger aggregation window, battery charge rate, pad size, and pad separation. Lastly, we leverage sensitivity results to form equations that approximate fleet and vertiport size and compare our results with previously published studies.

Overall Methodology

The fleet and vertiport sizing formulation in this paper relies on passenger flow data obtained with the discrete mode choice demand model and vertiport placement optimization framework that were developed as part of previous work, described in Kotwicz HERNICZEK and German, respectively (23, 24). For a given set of optimized vertiport locations and operational parameters, the mode choice demand model estimates the potential demand for a UAM commuting service based on the relative utility of available travel modes. More specifically, it estimates the daily number of commuters expected to utilize a UAM commuting service, their origins and destinations, and the vertiports through which their commutes are routed. Additional American Community Survey (ACS) data is necessary, however, to temporally distribute the demand data over a 24 h period and provide the passenger demand schedule used by the aircraft scheduling and vertiport sizing formulation. A breakdown of the fleet and vertiport sizing methodology is provided in Figure 1. Vertiport placement and passenger flow results from Kotwicz

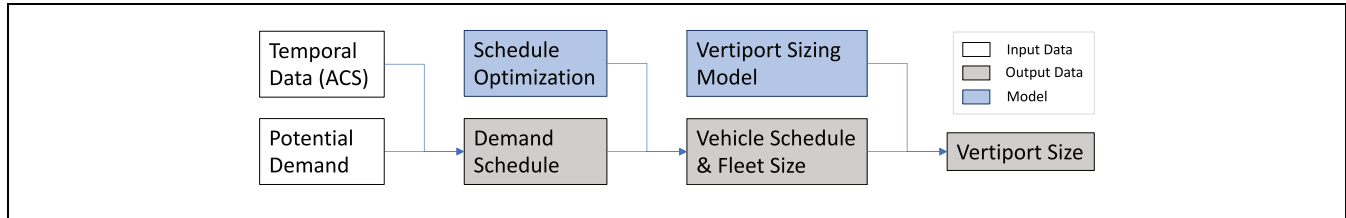


Figure 1. Fleet and vertiport sizing methodology flowchart.

Note: ACS = American Community Survey.

Herniczek and German, obtained for a UAM ticket price of \$5 + \$ 0.61/km and a service delay time of 5 min, are repeated in Figure 2 because of their relevance to fleet and vertiport sizing results presented throughout in the paper (24). It should be noted that: 1) the ranges of the color-bars among the subfigures of Figure 2 are not consistent, 2) regions of high demand are occasionally obscured by the vertiport icons (particularly in the Manhattan area within New York City), 3) demand flow values between vertiports are tabulated at the bottom of each subfigure, 4) demand flow is downsampled to 10,000 commuters per day to represent partially scaled-up, or mid-term operations, and to facilitate comparison of fleet and vertiport sizing results between cities, and 5) unless noted otherwise, presented results are based on demand flow and vertiport placement for the Atlanta combined statistical area (CSA), shown in Figure 2a. Weighted random sampling is used to sample the exhaustive list of origin-destination (OD) pairs associated with each region, with weights allocated based on the demand identified for each OD pair in Kotwicz Herniczek and German (24). To minimize the impact of sampling bias, the results presented in this paper are based on the average of the results obtained by sampling the geographic (Figure 2) and temporal (Figure 3) demand distributions 10 separate times. Additionally, error bars showing the range of values associated with the full set of sampled results are provided to demonstrate the effect of sampling bias.

Scheduling Methodology

Although the geographical distribution of potential demand (number of potential commuters) can be determined for every OD pair in a given region using the demand model described in Kotwicz Herniczek and German, it does not define the temporal distribution of that demand (23). Since we are modeling a commuting mission, we can estimate the temporal distribution using ACS data, and more specifically using Table B08302 and B23020, which provide the time of day that individuals leave home to go work, and the number of hours worked annually, at a tract level, respectively (25, 26). Note that: 1) we use the residential location (origin tract) to associate temporal ACS data to each OD pair, 2) we assume

the temporal distribution of departure times to be evenly distributed within block-groups of the same tract, and 3) we assume departure times to be uniformly distributed within binned increments. Additionally, the hours worked in a 12-month period provided by the ACS data are assumed to be evenly distributed over 250 workdays to estimate hours worked per day.

To obtain desirable vertiport departure times for commuters on their way to work, we add the time needed to reach the nearest vertiport ($t_{g,O \rightarrow V_O}$) to known departure times from home (t_O).

To obtain scheduling data for commuters on their way home from work, an estimate of the hours worked per day (t_{work}) is added to the time commuters arrive to work, where arrival time (t_D) is the sum of the departure time from home (t_O), the eVTOL flight time ($t_{e,V_O \rightarrow V_D}$), and the duration of the first and last ground-legs trips ($t_{g,O \rightarrow V_O}$ and $t_{s,V_D \rightarrow D}$), such that $t_D = t_O + t_{g,O \rightarrow V_O} + t_{e,V_O \rightarrow V_D} + t_{s,V_D \rightarrow D} + t_{work}$.

Likewise, to obtain vertiport departure times for commuters on their way home from work, we add the time needed to reach the nearest vertiport ($t_{s,D \rightarrow V_D}$) to the estimated departure time from work (t_D).

Note that subscripts O, D, V_O , and V_D refer to origin (home), destination (work), origin vertiport, and destination vertiport, respectively, and that subscripts g, e, and s refer to ground, eVTOL, and secondary modes of transportation, respectively. By applying this methodology to every OD pair, a schedule that identifies the desired departure time from vertiports to and from work is obtained for each commuter. The temporal distributions of desired vertiport departure times for the Atlanta, New York City, San Francisco, and Seattle CSA are illustrated in Figure 3.

Bilevel Rolling Window Fleet Scheduling Formulation

Given the geographical distribution of commuting demand obtained using the demand model and the temporal distribution of that demand, we can now find an aircraft schedule that minimizes the number of deadhead (repositioning) flights and minimizes the required fleet size. An optimal fleet size and schedule can be found nearly instantly for thousands of aircraft using a

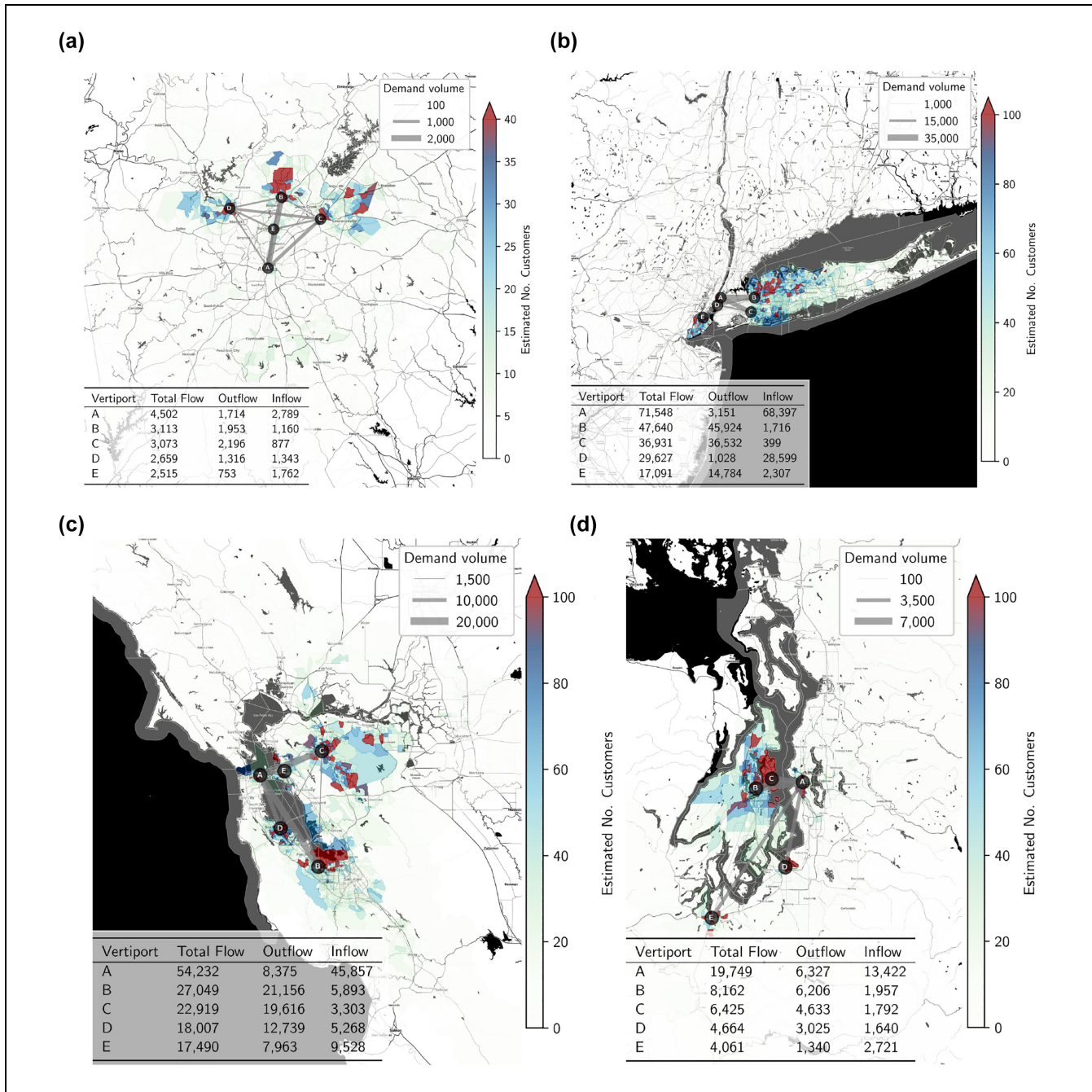


Figure 2. Vertiport placement optimization results for the Atlanta, New York City, San Francisco, and Seattle combined statistical areas (CSAs) from (24), obtained for a ticket price of \$5 + \$ 0.61/km and a service delay time of 5 min: (a) Atlanta CSA, (b) New York City CSA, (c) San Francisco CSA, and (d) Seattle CSA (24).

standard minimum-cost flow formulation by defining passenger-carrying departure and arrival times prior to optimization, thereby limiting the problem to optimization of repositioning flights.

In this work, the arrival time is defined as the sum of the departure time ($t_{\text{departure}}$) and flight time ($t_{e, V_O \rightarrow V_D}$), while the subsequent departure time ($t'_{\text{departure}}$) is the sum of the arrival time and the turnaround time

($t_{\text{turnaround}}$). We can therefore define the time that vehicles become available for subsequent flights as:

$$t'_{\text{departure}} = t_{\text{departure}} + t_{e, V_O \rightarrow V_D} + t_{\text{turnaround}} \quad (1)$$

where the turnaround time is the delay between the arrival and subsequent departure of a given vehicle and includes deplaning, taxiing, rotor spin-up and spin-down,

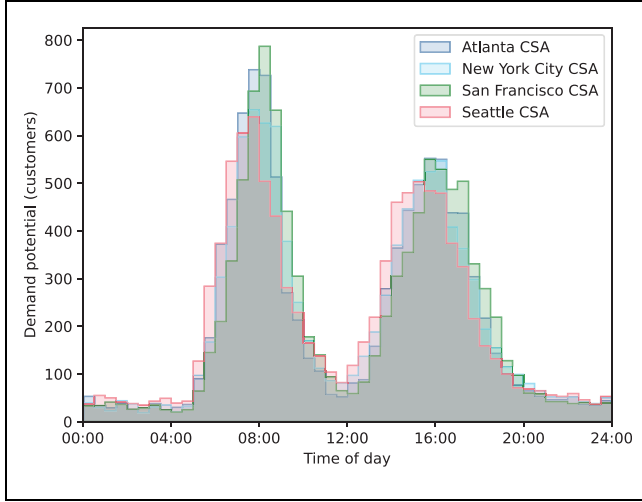


Figure 3. Potential demand distributed over 24 h based on regional American Community Survey (ACS) commuting data for the Atlanta, New York City, San Francisco, and Seattle combined statistical areas (CSAs) obtained for a ticket price of \$5 + \$ 0.61/km and a service delay time of 5 min (downscaled to 10,000 daily passengers).

boarding time, and battery charging or swapping time. In this work, we simplify the turnaround time in the scheduling formulation to the battery charge time under the assumption that the battery is charged an amount equivalent to the battery discharge after each flight and that a charging station is available on arrival. Battery charge time (t_{charge}) is calculated based on the ratio of the average eVTOL power consumption (P_{avg}) to battery charge rate (B_{charge}) and is given by:

$$t_{\text{charge}} = \frac{P_{\text{avg}} t_{e, V_O \rightarrow V_D}}{B_{\text{charge}}} \quad (2)$$

We then use a rolling window approach with an aggregation window of size Δt to aggregate commuter flow into vehicle flow prior to optimization. More specifically, once a passenger boards a flight, we assume that the aircraft will wait up to the aggregation window timespan if additional passengers are scheduled to arrive within the aggregation window. If the flight is full or if no additional passengers are scheduled to arrive within the remainder of the aggregation window then vehicles can be delayed up to the remainder of the aggregation window depending on flow conditions to limit spikes in the arrival and departure stream. This formulation behaves similarly to an on-demand scheduling approach where demand is known at least one aggregation window ahead of time, customers are guaranteed a wait time equal or lesser than the aggregation window, and all demand is guaranteed to be satisfied.

Upper-Level Objective: Fleet Size and Deadhead Flights. By modeling passenger-carrying (revenue) departures as sinks and modeling subsequent vehicle availability as sources of flow within the optimization model, we can formulate the fleet sizing and vehicle repositioning problem as the minimum-cost flow formulation given by Equations 3 to 6:

$$\text{Minimize } \omega \sum_q \sum_r f_{q,0 \rightarrow r} + \sum_t \sum_q \sum_{r \neq q} f_{q \rightarrow r, t} \quad (3)$$

$$\text{subject to } \sum_r f_{r \rightarrow q, t} + \psi_{q, t} = \sum_r f_{q, t \rightarrow r} \quad (4)$$

$$\sum_r f_{q, 0 \rightarrow r} = \sum_r f_{r \rightarrow q, t_n} \quad (5)$$

$$f_{q \rightarrow r, t} \in \mathbb{Z}^{0+} \quad (6)$$

where

$f_{q \rightarrow r, t}$ is an integer variable denoting the flow of aircraft between vertiports q and r , and q and r are subscripts that index the set containing all vertiport locations.

The objective function, given by Equation 3, is formed as a weighted sum, in which the first term represents the number of aircraft introduced into the network (fleet size), multiplied by a weighting factor ω , and the second term denotes all flows of aircraft between vertiports. Together, the two terms of the objective function minimize the fleet size and the total number of flights, thereby minimizing deadhead flights. In this work, a value of 100 is used for ω such that fleet size minimization is given priority within the objective function (note that a bilevel optimization formulation could be used rather than a weighted sum with a similar result). This is necessary because a cost is not associated to stationary aircraft parked at vertiports.

Equation 4 is applied to all vertiports q , and all times t , and has two roles: 1) enforcement of continuity on the flow of aircraft between vertiports, meaning that any aircraft in the network must either remain in place or fly to a linked vertiport in the network, and 2) introduction of flow sources and sinks using $\psi_{q, t}$, to model revenue flow between origin-destination pairs. The two-dimensional matrix representative of revenue flow, $\psi_{q, t}$, is formed a priori based on the known departure and arrival times of passengers and the number of seats per aircraft, as described earlier. Equation 5 is applied to all vertiports q , and ensures that the number of aircraft located at each vertiport at the start of each day matches the number of aircraft at the end of each day, such that the scheduling optimization results are applicable over multiple days (assuming the demand distribution remains similar). Lastly, Equation 6 is applied to all vertiports q, r , and all

times t , and limits values of aircraft flow to non-negative integers.

Lower-Level Objective: Vertiport Area. The baseline schedule optimization formulation given by Equations 3 to 6 does not directly minimize vertiport area, meaning that repositioning flights and stationary vehicles may not be optimal from a vertiport sizing perspective. For example, repositioning flights may unnecessarily occur during peak flow which will increase the number of vertiport pads required for arriving and departing flights. To resolve this limitation, vehicle scheduling can be optimized with vertiport area requirements as a secondary objective by using a bilevel optimization formulation. In this approach, the scheduling problem is first solved using the formulation described by Equations 3 to 6, and subsequently re-solved with a vertiport area objective and a constraint on fleet size, N_{aircraft} , and number of repositioning flights, $N_{\text{repositioning flights}}$, provided by the first optimization. If desired, the constraint on fleet size and repositioning flights can be relaxed with a relaxation factor, α , to give the optimizer greater flexibility to further reduce area, at the cost of a larger fleet size and more repositioning flights.

The structure of the vertiport area optimization is analogous to the scheduling formulation described above and is subject to the same constraints, that is, Equations 11 to 13. The area optimization formulation differs by the introduction of a minimax objective function, described by Equations 7 and 8, and by the addition of a constraint on fleet size, given by Equation 9, and a constraint on repositioning flights, given by Equation 10.

$$\text{Minimize } \sum_q A_q \quad (7)$$

$$\text{subject to } A_q \geq A_{q,t} \quad (8)$$

$$\sum_q \sum_r f_{q,0 \rightarrow r} \leq \alpha_1 N_{\text{aircraft}} \quad (9)$$

$$\sum_t \sum_q \sum_{r \neq q} f_{q \rightarrow r,t} \leq \alpha_2 N_{\text{repositioning flights}} \quad (10)$$

$$\sum_r f_{r \rightarrow q,t} + \psi_{q,t} = \sum_r f_{q,t \rightarrow r} \quad (11)$$

$$\sum_r f_{q,0 \rightarrow r} = \sum_r f_{r \rightarrow q,t_n} \quad (12)$$

$$f_{q \rightarrow r,t} \in \mathbb{Z}^{0+} \quad (13)$$

$$A_{q,t}, A_q \in \mathbb{R}^{0+} \quad (14)$$

where

$A_{q,t}$ is the area of vertiport q at time t , and A_q is the maximum area utilized by vertiport q over the schedule span (24 h).

The companion constraint given by Equation 8 is applied for all vertiports q and all times t , and is necessary to enforce a min-max objective, where Equation 8 ensures that A_q represents the maximum area of each vertiport over time, and the objective function Equation 7 pushes the maximum area values to be as small as possible. The methodology and formulations necessary to form $A_{q,t}$ are described in the subsequent section.

Despite the increased complexity of the area scheduling optimization formulation, it retains its linearity and remains well approximated by a continuous formulation. As a result, an optimal solution is generally obtained within several seconds or minutes. This formulation, with fleet size and number of flights constrained to the values obtained by Equations 3 to 6 without relaxation, is utilized to generate all vertiport sizing results provided in this paper.

Computational Efficiency

A significant benefit of this problem formulation is the scalability of the formulation with number of vertiports and number of vehicles. Since vehicles stationed at vertiports are represented as pools of vehicles, with flights to and from vertiports represented as arcs of flow that add or subtract vehicles from those pools (with a timespan equal to flight duration), there is no need to track vehicles individually. As a result, the number of variables and computational complexity scales with $t_n p^2$, where p is the number of vertiports in the network, and t_n in this case represents the number of time steps considered (assuming the worst-case scenario where vertiports form a complete network graph). As a result, a relatively large network of 100 vertiports and 144 time steps (10 min increments over a 24 h period) requires only 1,440,000 integer variables, regardless of the number of vehicles involved. Importantly, because the formulation inherently does not favor fractional flows, the problem is well approximated by a continuous linear programming formulation, significantly accelerating optimization of the integer programming formulation and enabling optimization within several seconds, even for this large problem size.

Model Limitations and Assumptions

Several assumptions and limitations are present in the formulation. Firstly, demand flows (revenue flights) are not directly optimized and are, instead, assigned prior to optimization. As a result, since demand is generated by sampling the demand distribution given by Figure 3, spikes in demand can occur for short intervals of time that increase fleet and vertiport size requirements. It should be noted, however, that revenue flights can be

directly optimized within a mixed integer linear programming formulation for the scale of problem presented in this work, but at an increased computational cost. A description and comparison of several scheduling methods, including a formulation that directly optimizes revenue flights and the rolling window formulation presented in this work, is provided in Kotwicz Herniczek (27).

Secondly, it is assumed that 100% of demand is satisfied within a given passenger aggregation window, which is expected to increase fleet and vertiport size requirements compared with formulations that allow for a fraction of demand to be rejected. Vehicles are also assumed to travel directly to their destinations, reducing opportunities for pooling of passengers. Given the time and energy sensitive nature of a UAM service, however, flights with intermediate stops are unlikely to provide a time saving to passengers and may suffer from reduced range or require recharging. As a result, flights with intermediate stops are unlikely for near-term operations. Additionally, parking capacity and vertiport throughput capacities are not enforced within the formulation but can be added if necessary by enforcing Equations 15 and 16 for each vertiport q at all times t :

$$f_{q \rightarrow q, t} \leq P_q \quad (15)$$

$$\sum_{r \neq q} f_{q \rightarrow r, t} + \sum_{r \neq q} f_{r \rightarrow q, t^*} \leq F_q \quad (16)$$

where

P_q = parking constraints unique to each vertiport, q , and

F_q = flow throughput constraints unique to each vertiport, q .

Note the use of t^* on the term $f_{r \rightarrow q, t^*}$ since arrival times need to be adjusted by $t_{\text{turnaround}}$ in order for Equation 16 to correctly denote departure and arrival flow. It should also be noted, however, that enforcement of capacity constraints may render the problem infeasible if the constraints are not reasonable relative to commuter throughput, unless the scheduling formulation allows for a portion of demand to be rejected.

Additionally, arc duration corresponding to block duration and turnaround time are based on the summation of direct flight distances with a flight speed of 300 km/h and the time necessary to recharge the battery to 100% after each flight. It should be noted that this assumption increases fleet size requirements compared with a scenario where aircraft are only being fully recharged during off-peak periods and limited fast-charging occurs during peak periods as necessary.

Charging infrastructure is assumed to always be available, meaning that all vehicles are assumed to begin charging on arrival. Furthermore, the power consumption limitations of the charging infrastructure are not

considered when calculating recharge time, meaning that fleet size may be underestimated if large vertiports exist in the vertiport network where many vehicles need to charge simultaneously. These two simplifications could be addressed by the addition of explicit gate nodes within the network flow model.

Lastly, no additional provisions are made for taxiing time, transition flight, indirect trajectories, or passenger loading. It should be noted, however, that these durations can easily be added to the model as long as they are consistent across OD pairs or known for every OD pair prior to optimization, since they only modify arc durations and do not add complexity to the formulation.

Vertiport Sizing Methodology

In this work, we consider a minimalist vertiport topology composed of four types of area: pad areas, pad clearance areas, gate areas, and parking areas. “Pad area” denotes the surface used for liftoff and touchdown, “pad clearance area” is the area between pads required for simultaneous independent operations, “gate area” is the preparation area used for battery charging and passenger embarking and disembarking (similar in function to airport gates), and, lastly, “parking area” refers to the area required to station eVTOL vehicles not currently in use. Given that a lower bound on vertiport area is desired, we assume that: 1) pad clearance areas can be used as vertiport parking and gate areas, and 2) pad areas can be dynamically repurposed to parking areas if the pad is not in use. With these assumptions, we can define the minimum vertiport area for operations at vertiport q at a given time t within the optimized vehicle schedule obtained from the extended scheduling formulation as:

$$A_{q, t} = A_{\text{pad}, q, t} + \max(A_{\text{clearance}, q, t}, A_{\text{parking}, q, t} + A_{\text{gate}, q, t}) \quad (17)$$

and the minimum vertiport area to sustain all scheduled operations at vertiport q to be:

$$A_q = \max_t A_{q, t} \quad (18)$$

The total pad, gate, and parking area can each be defined as the product of a single pad, gate, or parking area, and the number of pads, gates, and parking areas, respectively. The total clearance area can also be approximated in this manner, but a more accurate definition requires a description of the topology and is provided later, in Equation 32.

$$A_{\text{pad}, q, t} = N_{\text{pads}, q, t} A'_{\text{pad}} \quad (19a)$$

$$A_{\text{gate}, q, t} = N_{\text{gates}, q, t} A'_{\text{gate}} \quad (19b)$$

$$A_{\text{parking}, q, t} = N_{\text{park}, q, t} A'_{\text{parking}} \quad (19c)$$

$$A_{\text{clearance}, q, t} \approx N_{\text{pads}, q, t} A'_{\text{clearance}} \quad (19d)$$

Using the optimized schedule, we can define the number of gates and pads required at vertiport q over time step t as a function of the number of arrivals and departures to and from vertiport q over that time step, $f_{q=r, t}$. Likewise, we can define the number of parking areas required at vertiport q over time step t as the number of vehicles that remain in place at vertiport q over that time step, $f_{q \rightarrow q, t}$. If the pad throughput (f_{pad}), defined as the number of arrivals and departures that a single vertiport pad can process within one time step, is greater than one, we can define the number of pads as:

$$N_{\text{pads}, q, t} = \left\lceil \frac{f_{q=r, t}}{f_{\text{pad}}} \right\rceil \quad (20)$$

Note the use of ceiling $\lceil x \rceil$ function notation to ensure that we have a sufficient integer number of vertiport pads, gates, and parking locations for a given flow and throughput of vehicles. Also, note that if pad or gate throughput are much greater than one, Equations 20 and 21 only hold if the distribution of arrivals and departures for adjacent time increments remain similar. For example, if we use a large time increment of 10 min and assume that arrivals and departures are uniformly distributed over that time increment, then the arrival and departure stream must remain relatively uniform over subsequent time steps. Otherwise, the required number of pads and gates will be underestimated.

The same pattern is repeated for the number of gates if the gate throughput ($f_{\text{gateIN}}, f_{\text{gateOUT}}$) is greater than one, although a distinction is necessary for inflow and outflow, since gates associated with inflow are also responsible for vehicle charging.

$$N_{\text{gates}, q, t} = \lceil N_{\text{gatesIN}, q, t} + N_{\text{gatesOUT}, q, t} \rceil \quad (21a)$$

$$N_{\text{gatesIN}, q, t} = \frac{f_{r \rightarrow q, t}}{f_{\text{gateIN}}} \quad (21b)$$

$$N_{\text{gatesOUT}, q, t} = \frac{f_{q \rightarrow r, t}}{f_{\text{gateOUT}}} \quad (21c)$$

Lastly, the number of required parking areas is equal to the number of vehicles remaining stationary at each vertiport over a given time step:

$$N_{\text{park}, q, t} = f_{q \rightarrow q, t} \quad (22)$$

In the case that pad (f_{pad}) or gate throughput ($f_{\text{gateIN}}, f_{\text{gateOUT}}$) is less than one, however, we must consider the flow of vehicles in neighbouring time periods, since infrastructure usage during previous time periods spill over

into the current time period being considered. For example, imagine that we have 10 aircraft that need charging infrastructure at a given time step and that charging lasts two time periods. If five additional aircraft began charging in the previous time step, then we need a total of 15 gates to accommodate aircraft from the current and previous time period. The number of previous time periods that must be considered is defined by f_{pad}^{-1} . To generalize the notation to deal with cases where f_{pad}^{-1} is a fractional number, then we must consider infrastructure usage from previous $\lfloor f_{\text{pad}}^{-1} - 1 \rfloor$ time periods as well as fractional infrastructure usage given by $\{f_{\text{pad}}^{-1}\} f_{q=r}$ at time period $t - \lfloor f_{\text{pad}}^{-1} \rfloor$. To shorten Equations 23, 24a, and 24b we introduce the notation τ_{pad} to represent $\lfloor t - f_{\text{pad}}^{-1} \rfloor$. With this notation, we can define the number of pads and gates for cases where pad or gate throughput is less than one as:

$$N_{\text{pads}, q, t} = \left\lceil \{f_{\text{pad}}^{-1}\} f_{q=r, \tau_{\text{pad}}} + \sum_{\tau_{\text{pad}}+1}^t f_{q=r, t} \right\rceil \quad (23)$$

$$N_{\text{gatesIN}, q, t} = \{f_{\text{gateIN}}^{-1}\} f_{r \rightarrow q, \tau_{\text{gateIN}}} + \sum_{\tau_{\text{gateIN}}+1}^t f_{r \rightarrow q, t} \quad (24a)$$

$$N_{\text{gatesOUT}, q, t} = \{f_{\text{gateOUT}}^{-1}\} f_{q \rightarrow r, \tau_{\text{gateOUT}}} + \sum_{\tau_{\text{gateOUT}}+1}^t f_{q \rightarrow r, t} \quad (24b)$$

Vehicle inflow, $f_{r \rightarrow q, t}$, outflow, $f_{q \rightarrow r, t}$, and total throughput, $f_{q=r, t}$, can be more formally defined as:

$$f_{r \rightarrow q, t} = \sum_{\substack{r \\ r \neq q}} f_{r \rightarrow q, t^*} \quad (25)$$

$$f_{q \rightarrow r, t} = \sum_{\substack{r \\ r \neq q}} f_{q \rightarrow r, t} \quad (26)$$

$$f_{q=r, t} = f_{r \rightarrow q, t} + f_{q \rightarrow r, t} \quad (27)$$

where the use of t^* on the term $f_{r \rightarrow q, t^*}$ is necessary because arrival times need to be adjusted by $t_{\text{turnaround}}$ in order for Equations 25 to 27 to correctly denote departure and arrival flow over time step t .

Pad and gate throughput, which represent the number of vehicles that a pad and gate can process per discrete time increment, Δt_s , is a function of both the time increment and the time required for the pad and gate to process a single vehicle, respectively:

$$f_{\text{pad}} = \frac{\Delta t_s}{t_{\text{pad}}} \quad (28a)$$

$$f_{\text{gateIN}} = \frac{\Delta t_s}{t_{\text{gateIN}}} \quad (28b)$$

$$f_{\text{gateOUT}} = \frac{\Delta t_s}{t_{\text{gateOUT}}} \quad (28c)$$

Here, pad clearance time (t_{pad}) includes the time required to clear the approach or departure surface and the taxiing time near the pad. The gate time for outgoing passengers (t_{gateOUT}) includes the time required to disembark, rotor spin-down time, and taxiing time near the gate. Lastly, the gate time for incoming passengers (t_{gateIN}) is assigned the greater of 350s or battery charging time, and also includes disembarking, taxiing, and rotor spin-down time.

Pad sizing in this work is based on pad sizing guidelines published by the FAA and vertiport topology is based on final approach and take-off (FATO)–FATO separation requirements for simultaneous independent helicopter operations (9, 28). The relationship between the touchdown and lift-off area (TLOF), FATO, and pad safety area are illustrated in Figure 4, where D is the maximum vehicle size, defined as the diameter of the smallest circle enclosing the eVTOL aircraft projected on a horizontal plane while the aircraft is in the take-off or landing configuration with rotor(s) turning (10).

From Figure 4, the area requirements per pad can be defined as:

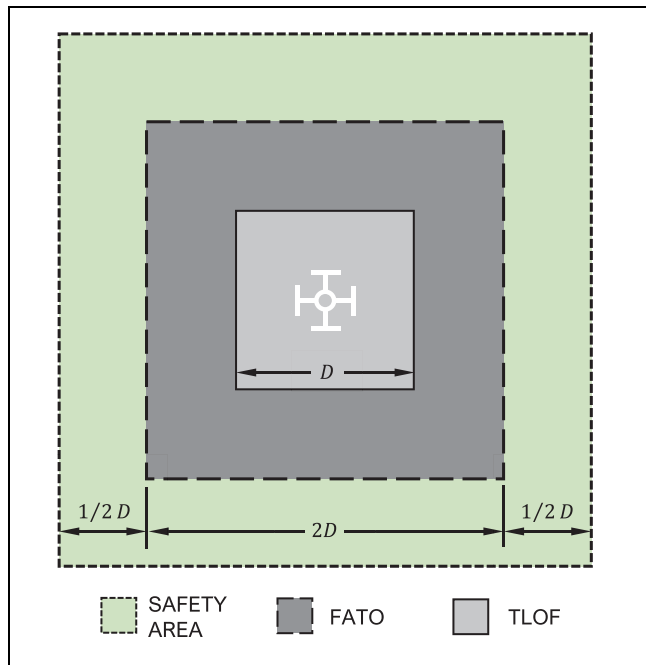


Figure 4. Vertiport pad design.

Note: D = maximum vehicle size; FATO = final approach and take-off; TLOF = touchdown and lift-off area.

Source: Adapted from Meyers (9).

$$A'_{\text{pad}} = 9D^2 \quad (29)$$

Since we are aiming to find the minimum vertiport area required for a given vehicle schedule, we assume that eVTOL parking and gate areas are defined by the vehicle footprint, D , and are therefore equal to the TLOF area:

$$A'_{\text{parking}} = A'_{\text{gate}} = D^2 \quad (30)$$

Although smaller area requirements may be possible using staggered vehicle formations or vehicles with folding wings, these are not considered, to maintain the simplicity of the formulation.

Lastly, a compact, linear vertiport topology, illustrated in Figure 5, is considered to minimize the vertiport area required to support a given throughput. To maximize throughput and reduce area requirements, vertiport FATOs are separated by 61 m (200 ft) in accordance with requirements for heliports supporting simultaneous independent operations. It should be noted that this topology was created only with space efficiency in mind to create a lower bound on vertiport area requirements and does not consider limitations related to footprint aspect ratio, gate–pad connectivity, nor taxiway area and placement.

Using the topology defined by Figure 5, we can finally define the approach and departure clearance area associated with each pad (in meters) as:

$$A'_{\text{clearance}} = 3D(61 - D) \quad (31)$$

and fully describe the total required clearance area as:

$$A_{\text{clearance}, q, t} = (N_{\text{pads}, q, t} - 1)A'_{\text{clearance}} \quad (32)$$

where $N_{\text{pads}, q, t} - 1$ takes into consideration that clearance is required only between vertiport pads; for example, a two-pad design requires only a single clearance space. Note the conversion from 200 ft to 61 m in Equation 31.

Model Limitations and Assumptions

Several significant assumptions and limitations are inherent to the vertiport sizing methodology; namely the aspect ratio of the linear vertiport topology becomes very large as the number of pads increases. Although this leads to footprints that may be unrealistic for large vertiports placed near city centers, the estimated area remains valid as a lower bound, which is the goal of this methodology.

Several simplifications are also made to the vertiport design, including omission of taxiways, charging infrastructure area, safety margins on gates and parking areas, and the lack of consideration of approach and departure stream complexity. Emergency landing contingencies, that may require dedicated areas or prevent vertiports

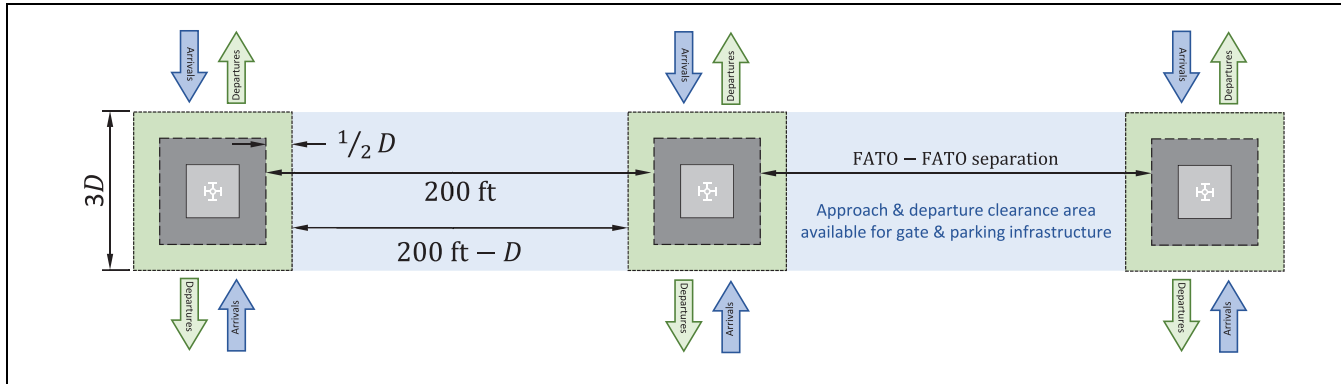


Figure 5. Compact linear vertiport topology with three pads capable of simultaneous independent operations.

Note: D = maximum vehicle size; FATO = final approach and take-off.

from running at maximum capacity for prolonged periods of time, are also not considered. Likewise, although these omissions reduce the accuracy of the estimated vertiport area, they solidify the sizing estimate as a lower bound on required vertiport area.

Exotic multi-level vertiport designs with parking areas, pads, or gates spread across multiple floors are an important exception to the validity of the estimated area as a lower bound but are unlikely to be implemented in the near-term. It should be noted, however, that the vertiport area results in this work are valid only as a lower bound compared with other topologies or sizing methodologies if operational and vehicle parameters relevant to vertiport sizing are consistent between methodologies. Additionally, operational constraints related to airspace management, such as the influence of existing air traffic on pad throughput, are not considered. The fleet of aircraft using the vertiport network is also assumed to be homogeneous, meaning that vehicle and operational parameters such as pad size, pad throughput, and aircraft passenger capacity are uniform throughout the vertiport network.

It should be noted that the omission of charging infrastructure limitations from the sizing model may lead to underestimation of gate and parking infrastructure requirements for large vertiports but is not expected to significantly influence vertiport sizing requirements. This is because power output limitations restrict the number of vehicles that can charge simultaneously, thereby reducing the number of gates (and area) that can be used for charging but increasing the area required to park aircraft as they wait for gates to become available. This leads to an increase in turnaround time which increases fleet size and thereby also increases parking area requirements. We do not expect this simplification to significantly influence the vertiport sizing requirements obtained in this work, however, because we found vertiport area to generally be driven by pad area requirements.

Conversely, the assumption that turnaround time is equal to the time necessary to recharge the battery to 100% after each flight is expected to overestimate fleet size and gate area requirements compared with a scenario where aircraft are only fully recharged during off-peak periods and limited fast-charging occurs during peak flow periods as necessary. Likewise, this assumption is not expected to significantly influence vertiport sizing requirements because vertiport area was found to generally be driven by pad area requirements.

Lastly, temporal factors such as per-passenger boarding and disembarkation times are neglected because of their relatively low time requirements (7). Differences between boarding and disembarking, and between approach and departure times, likewise could be considered but are neglected to maintain model simplicity.

FAA versus EASA Guidelines and Industry Perspective

In this work, we utilize FAA guidance on vertiport design as the baseline for vertiport pad dimension and FATO–FATO separation. As shown in Table 1, however, vertiport sizing guidelines prescribed by the FAA are significantly more conservative than FAA general aviation (GA) heliport and EASA vertiport guidelines. As a result, aviation associations and technical societies (including Aerospace Industries Association, General Aviation Manufacturers Association, Helicopter Association International, National Business Aviation Association, and the Vertical Flight Society) have responded to the FAA’s published vertiport guidelines, stating that the FATO sizing guidelines are overly prescriptive and conservative given that UAM vehicles are anticipated to have capabilities similar to, or better than, helicopters during takeoff and landing. They have recommended that the sizing guidelines align with either EASA’s vertiport guidelines or FAA’s GA heliport sizing guidelines (29).

Table 1. Comparison of Vertiport Sizing Guidelines

Parameter	FAA GA heliport (28)	EASA vertiport (10)	FAA vertiport (9)
TLOF width & length or diameter	0.83 D	0.83 D	1 D
FATO width & length or diameter	1.50 D	1.50 D	2 D
Safety area width	Max. (0.28 D , 20 ft)	Max. (0.25 D , 10 ft)	0.5 D
FATO–FATO separation ^{1,2}	61 m (200 ft)	60 m (197 ft)	not specified

Note: D = maximum vehicle size; EASA = European Aviation Safety Agency; FAA = Federal Aviation Administration; FATO = final approach and take-off; GA = general aviation; Max. = maximum; TLOF = touchdown and lift-off area.

¹Separation distance for simultaneous independent operations (takeoffs and landings).

²EASA guidelines do not specifically define a FATO–FATO separation distance for electric vertical take-off and landing aircraft but refer to 60 m as a recognized guideline for helicopter operations (10).

By following EASA's vertiport sizing guidelines, and reducing the FATO and safety area width from $2D$ and $0.5D$ to $1.5D$ and $0.25D$, respectively, the required area for vertiport infrastructure can be reduced by 33% to 50% depending on the number of pads and assuming the pad topology depicted in Figure 5. A reduction in pad separation, however, has a less predictable impact on vertiport area, since reducing pad separation also reduces clearance area that is shared with gate and parking areas. In this work, we found that a reduction in pad separation below 125 ft does not reduce overall vertiport area with the baseline scheduling and vertiport parameters. It should be noted, however, that this threshold shifts if the vertiport composition (number of pads, gates, and parking spots) or vertiport topology changes, or if pad clearance area cannot be utilized for gate operations or as parking space.

To further explore the influence of changes to FATO width and FATO–FATO separation distance for simultaneous independent operations, we consider a range of values for each of these parameters that includes FAA and EASA vertiport guidance. Note that a linear relationship between safety area and FATO width is assumed such that a safety area of 0 , $0.25D$, $0.5D$ corresponds to a FATO width of $1D$, $1.5D$, and $2D$, the latter two of which coincide with EASA and FAA guidance, as shown in Table 1.

Vertiport Scheduling and Sizing Parameters

Vertiport sizing is heavily influenced by scheduling-related parameters such as daily passenger volume, passenger capacity, and battery charging time, in addition to sizing-specific parameters such as vertiport topology, vehicle size, and the throughput of individual pads and gates. The baseline value and ranges used for each of these parameters in the sensitivity analysis are provided in Table 2.

The range considered for number of passengers and for vehicle size are based on existing eVTOL concepts,

where it should be noted that vehicle passenger capacity is an input to the scheduling optimization model rather than the sizing model (5). Pad and gate times are based on Preis and Hornung, where it should be noted that gate tasks such as boarding, deplaning, and rotor spin-up and spin-down are assumed to occur within 90 s and 350 s, respectively (7). Lastly, battery charging time is a function of the charge rate and is defined using a simple energy model by Equation 2, where the average eVTOL power consumption (P_{avg}) is based on estimates for existing vehicle designs, and the chosen battery charge rate range (B_{charge}) is based on 100% to 150% of existing electric-car fast-charging capabilities to consider both existing and near-term battery technologies (30–33).

Results and Discussion

Scheduling and vertiport sizing results were obtained using the parameters provided in Table 2. Unless specifically mentioned otherwise, results were obtained for the Atlanta–Athens–Clarke County–Sandy Springs, GA CSA using a rolling window scheduling approach described by Equations 3–8 and 14. The baseline vehicle and operational parameters defined in Table 2, that is, a vehicle size of 15 m (50 ft), a vehicle passenger capacity of four, a passenger aggregation window of 600 s (10 min), a pad clearance time of 90 s, a battery charge rate of 200 kW, a pad dimension of $3D$, and a FATO–FATO separation distance of 200 ft, are used for all results, with the exception of sensitivity studies specific to those parameters.

The Results and Discussion section is ordered as follows. We first present sizing results for a vertiport network in Atlanta to demonstrate the behavior of the vertiport sizing formulation and to explore the impact of vertiport sizing requirements on UAM commuting service scalability. We then compare the sensitivity of fleet and vertiport sizing results with regional variations in the temporal and geographic distribution of demand for the Atlanta, New York City, San Francisco, and Seattle

Table 2. Vertiport Scheduling and Sizing Parameters

Parameter	Description	Range	Baseline value
demand ¹	passengers per day	100–10,000	10,000
D	maximum vehicle size	5–15 m	15 m (50 ft)
n_{pax}	vehicle passenger capacity	2–8	4
Δt	passenger aggregation window	300–1,800 s	600 s (10 min)
Δt_s	scheduling formulation time increment	na	60 s
t_{pad}	pad clearance time required per aircraft	20–120 s	90 s
t_{gateOUT}	gate time required per outbound aircraft	na	100 s
t_{gateIN}	gate time required per inbound aircraft	na	Max. (350 s, t_{charge})
B_{charge}	battery charge rate	100–400 kW	200 kW
P_{avg}	avg. aircraft power consumption	na	300 kW
pad dimension	total pad dimension (FATO + safety width)	1–3 D	3 D
pad separation ²	FATO–FATO separation distance	D –61 m	61 m (200 ft)

Note: FATO = final approach and take-off; Max. = maximum; na = not applicable.

¹Demand is not strictly an input parameter to the scheduling formulation but is used to sample the temporal demand distribution and generate a commuter demand schedule.

²A minimum FATO–FATO separation of D ensures that safety areas do not overlap (following Federal Aviation Administration vertiport guidelines).

CSAs. Lastly, we present sensitivity results for the parameter ranges provided in Table 2, including demand, battery charging rate, aircraft passenger capacity, pad clearance time, vehicle dimension, FATO width, and FATO–FATO separation.

It should be noted that error bars are included in the results presented below because of the sensitivity of sizing results on sampling of the geographic and temporal demand distributions (Figures 2 and 3). To address this, each sensitivity study was repeated 10 times, and the mean of the results are plotted, along with error bars showing the minimum and maximum values obtained. Also note that “vertiport network area” refers to the summation of the areas allocated to each individual vertiport in the network, and that “vertiport composition” refers to distribution of pads, gates, and parking infrastructure in the vertiport network.

Atlanta Scheduling Results

Results from the scheduling optimization formulation for the Atlanta region illustrating the overall utilization and load factor of vehicles and the distribution and flow of vehicles across the vertiports of the network are presented in Figures 6 and 7, respectively. Scheduling optimization for the Atlanta region converged to a fleet size of 121 vehicles, and required 3,296 revenue flights and 373 deadhead repositioning flights to fulfill a volume of 10,000 passengers over a 24 h period. Note that the results presented in this section correspond to an aggregation window of 10 min and that turnaround time is calculated for a vehicle power consumption of 300 kW, and a battery charge rate of 200 kW. Also note that a daily volume of 10,000 passengers corresponds to 5,000 commuters flown from home to work (generally in the

morning) and from work to home (generally in the evening). These fleet sizing results correspond to about 30 flights per vehicle per day, an average passenger load factor of 70%, and an average of 83 passengers transported per aircraft per day.

As expected, aircraft utilization, shown in Figure 6, follows the temporal demand distribution given in Figure 3. Likewise, the passenger load factor of revenue flights is higher during periods of high demand because of increased opportunity for passenger aggregation; however, the overall load factor during peak flow periods is reduced by an associated increase in necessary repositioning deadhead flights. We can also observe that a significant fraction of the fleet requires charging during peak demand because of the use of a low battery charge rate (200 kW) relative to the vehicle power consumption (300 kW). This charge-to-consumption ratio effectively means that a 10 min flight will require 15 min of charging time. As expected, aircraft utilization nears 100% during peak demand periods.

Analysis of Figures 2a and 7 shows that demand flow is not balanced between vertiports or throughout the day. In particular, vertiport A (and E to a lesser extent) experience significantly higher inflow of aircraft during the morning commuting peak (6:00–9:00 a.m.), whereas vertiport C (and B to a lesser extent) experience more outflow during the same time period. This is because of vertiports A and E being located more centrally, thereby acting as workplace hubs, as shown in Figure 7, compared with vertiports B, C, and D, which are located in the Atlanta suburbs and primarily serve as residential hubs. This trend reverses in the evening when commuters return home from work. As a result of imbalanced flow, significant parking infrastructure is needed during off-peak periods and repositioning

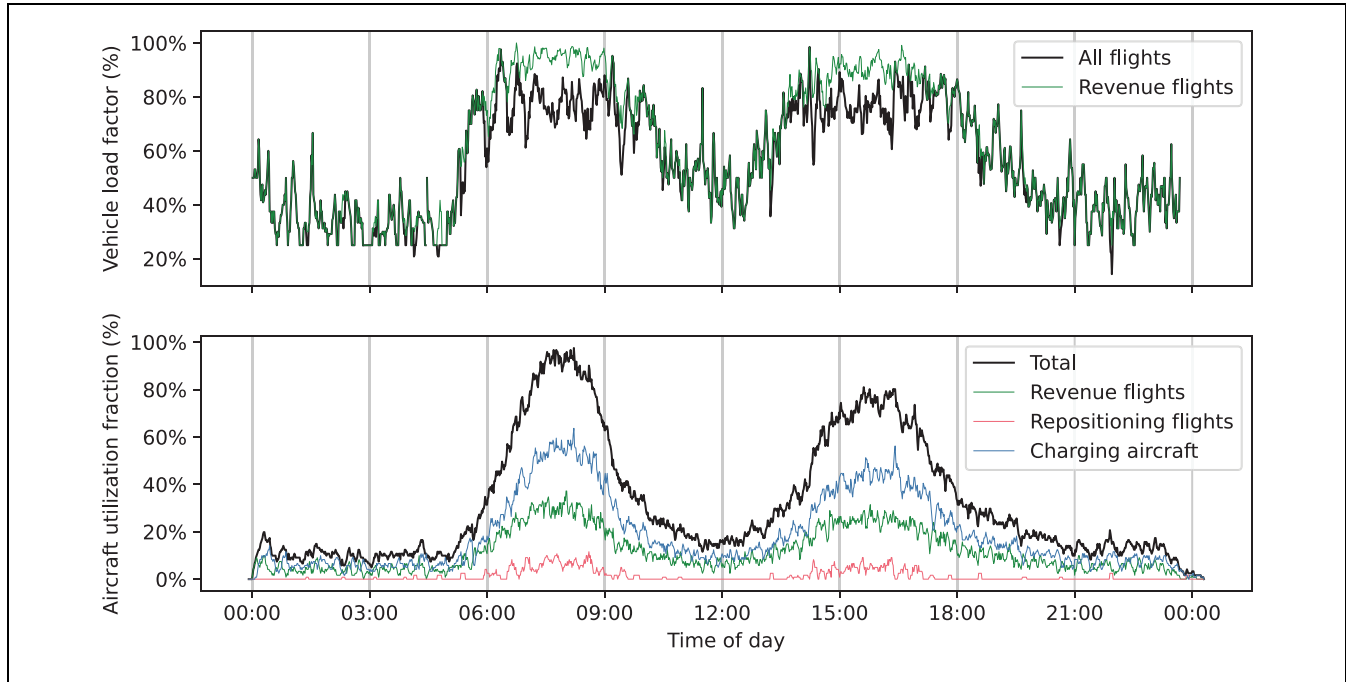


Figure 6. Vehicle load factor (top) and utilization (bottom) over a 24 h period for a vertiport network in the Atlanta region (160 vehicle fleet-size; four passenger vehicle capacity).

flights are needed to ensure that demand can be served during peak periods.

Atlanta Vertiport Sizing Results

Vertiport-network sizing results for the Atlanta region are presented in Table 3. A sizeable land-footprint of 10.7 ha (26.4 acres) is required for the network of vertiports in this example, with the largest vertiport in the network requiring an area of 3.1 ha, and a maximum of 8 pads, 30 gates, and 77 parking spots over 24 h. These results suggest that the demand concentration per vertiport in this example may be more suitable for industrial and rural areas where large parcels of land and large flat rooftops are more common, rather than dense urban areas, unless operations for a given vertiport can be partitioned over a cluster of several smaller vertiports. The area requirement of 3.1 ha for the largest vertiport is particularly problematic because it is located in Atlanta's downtown core and may limit the scalability of UAM operations. Results also suggest that parking area (and likely gate area if charging times are long) may be a substantial portion of the vertiport footprint if vertiport areas cannot be repurposed throughout the day or if clearance area is reduced.

Given the large land area requirement for scaled-up UAM operations, and the nonuniform and imbalanced nature of commuting demand, it is anticipated that smaller-scale UAM commuting operations that focus on

providing a transportation service that replaces helicopter, float plane, or ferry operations to be more feasible in the near term. Alternatively, commuting operations that bring passengers from the suburbs to a metro hub rather than directly to the downtown core may alleviate land-use problems. Likewise, focusing on transportation with more stable demand, such as an airport air taxi mission, may also be more practical in the near term. Regardless, large-scale UAM operations will likely require higher-passenger-density vehicles, or novel vertiport concepts that do not align with current FAA and EASA guidance.

Note that the sum of pad, gate, and parking area is not equal to the vertiport area because we assume that pad clearance area can be used as gate and parking areas and because dynamic repurposing of the vertiport surfaces is allowed, meaning, for example, that unused vertiport pads in off-peak periods can be used as parking space if necessary. This dynamic repurposing can be observed in Figure 8, which illustrates vertiport usage requirements throughout the day for Vertiport A from Figure 7. We can observe that vertiport area requirements are driven by pad area requirements during the morning commuting demand peak and that the imbalance of flow leads to a substantial repurposing of pad and clearance area into parking area during midday, off-peak operations. We can also observe that sufficient clearance area exists during peak flow such that gate and parking area does not add to the total area requirement. It should also be noted that these vertiport sizing results

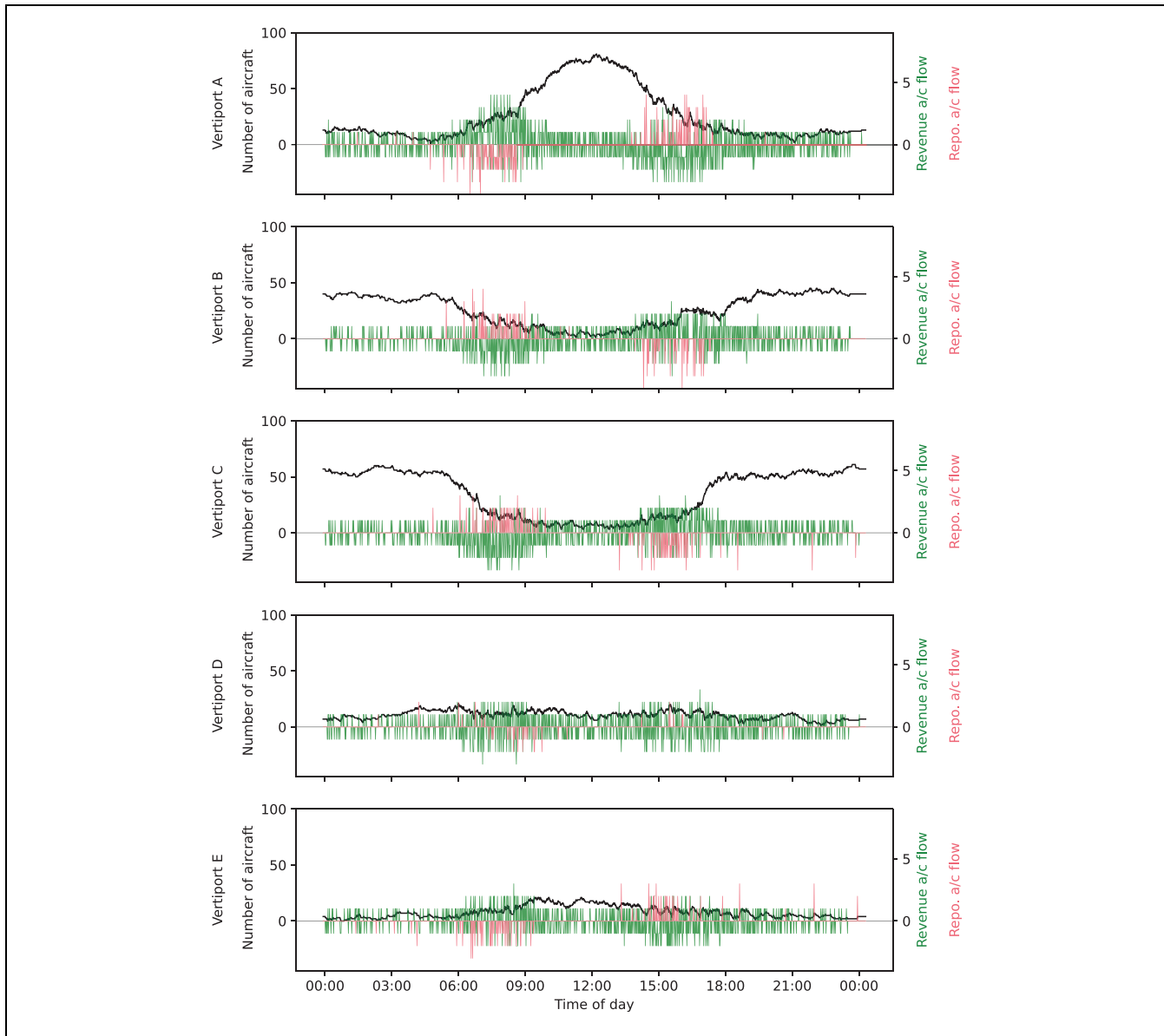


Figure 7. Distribution and flow of vehicles across a network of five vertiports (A–E) in the Atlanta region over a 24 h period. Note: a positive aircraft (a/c) flow on the secondary axis refers to an inflow of vehicles at that vertiport.

correspond to a fleet size of 121 vehicles, 3,669 revenue flights, and 373 repositioning flights.

Region-Based Results

Region-based scheduling and vertiport sizing results for the CSAs associated with Atlanta, New York City, San Francisco, and Seattle for a normalized daily volume of 10,000 passengers are presented in Figure 9. From Figure 9a, we see that the total number of flights are not consistent across each region, even though revenue flights are defined prior to optimization and are largely a function

of demand flow, the sum of which is enforced to be consistent between regions in this comparison.

These variations are primarily driven by differences in demand-flow balance. We can observe in Figure 2, for example, that the vast majority of demand in New York City is for trips into vertiport A (for a morning commute), located in Manhattan. As a result, significantly more repositioning flights are necessary compared with Atlanta, where most vertiports experience a more balanced flow of vehicles throughout the day, as shown in Figure 9b. Interestingly, New York City features the highest revenue load factor (Figure 9c) of the considered

Table 3. Vertiport Sizing Results for the Atlanta Region

Parameter	Vertiport network	Largest vertiport ¹
Required vertiport area	10.7 ha	3.1 ha
Required pad and clearance area ²	10.6 ha	3.1 ha (8 pads)
Required gate area ²	2.4 ha	0.7 ha (30 gates)
Required parking area ²	5.0 ha	1.8 ha (77 parked aircraft)

¹Refers to the central vertiport labeled as vertiport A in Figures 2 and 7.

²Areas are individually maximized over time and consequently do not sum to vertiport area since all areas can be dynamically repurposed as necessary.

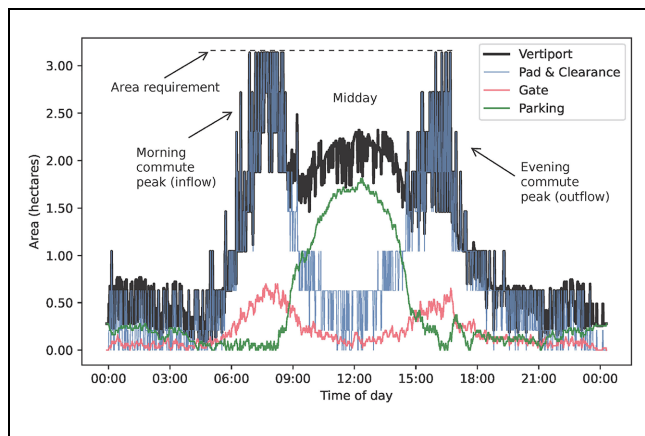


Figure 8. Vertiport sizing requirement timeline for the largest vertiport in the Atlanta network (labeled as Vertiport A in Figures 2 and 7).

regions because of a more concentrated demand flow (as shown in Figure 2), meaning that passengers can more easily be aggregated. Given that repositioning flights are deadhead flights, however, (meaning that no passengers are onboard), the higher repositioning flight fraction of New York City leads it to have the lowest network load factor of the considered regions as shown in Figure 9d. Atlanta suffers from the opposite effect and features the lowest revenue load factor but highest network load factor because of a less concentrated but more balanced demand distribution.

Moving on to fleet size sensitivity, shown in Figure 9e, we can observe that fleet size is similar for most regions, with the exception of San Francisco which requires a significantly larger fleet for a given demand. This was found to be a result of two contributing factors. First, the longer average flight distance between vertiports in the San Francisco region, shown in Figure 9f, causes a larger portion of the San Francisco fleet to be unavailable during peak demand flow conditions, meaning that a larger fleet

size is necessary to meet demand for a given aggregation window. This effect is compounded because longer flights consume more energy which results in longer vehicle charging durations. Second, San Francisco experiences a higher concentration of demand during the morning commuting peak, as demonstrated in Figure 3. This, in turn, increases fleet size requirements, since fleet size is determined by peak flow conditions. On the other hand, although the vertiport locations in New York City have the shortest average flight distance and a slightly less concentrated peak demand, a smaller fleet size is not observed for New York City because of its larger number of flights and associated lower overall load factor, which also have an impact on fleet size.

Lastly, comparing vertiport area requirements illustrated in Figure 9g, which are also influenced by peak flow conditions, it can be observed that the necessary vertiport area generally correlates with the number of flights required. As will be shown later, this is a result of vertiport area being primarily driven by the required number of pads and is a consequence of our assumption that gates and parking spots can be placed within the pad clearance area. San Francisco slightly deviates from this trend because of its elevated demand concentration during peak commuting hours which results in a greater number of pads. Although the fleet size for each region in Figure 9e is not unreasonable for a daily volume of 10,000 passengers, the vertiport network area requirement poses a bigger challenge because a significant portion of the vertiport network area requirement corresponds to vertiports located in dense urban areas of each city, specifically, the Atlanta Downtown core, Seattle Central Business District, San Francisco Financial District, and Central Manhattan. A potential solution would be to partition demand over a cluster of smaller nearby vertiports rather than a single centralized vertiport. This approach, however, risks increasing airspace and fleet balancing complexity.

Sensitivity Results

Sensitivity results for the parameter ranges provided in Table 2, including demand, battery charging rate, aircraft passenger capacity, pad clearance time, vehicle dimension, FATO width, and FATO–FATO separation, are presented below. The reader is reminded that a vehicle size of 15 m (50 ft), a vehicle passenger capacity of four, a passenger aggregation window of 600 s (10 min), a pad clearance time of 90 s, a battery charge rate of 200 kW, a total pad dimension of 3D (150 ft), and a FATO–FATO separation distance of 200 ft are used for all results, with the exception of sensitivity studies specific to those parameters. Findings presented in this section were obtained

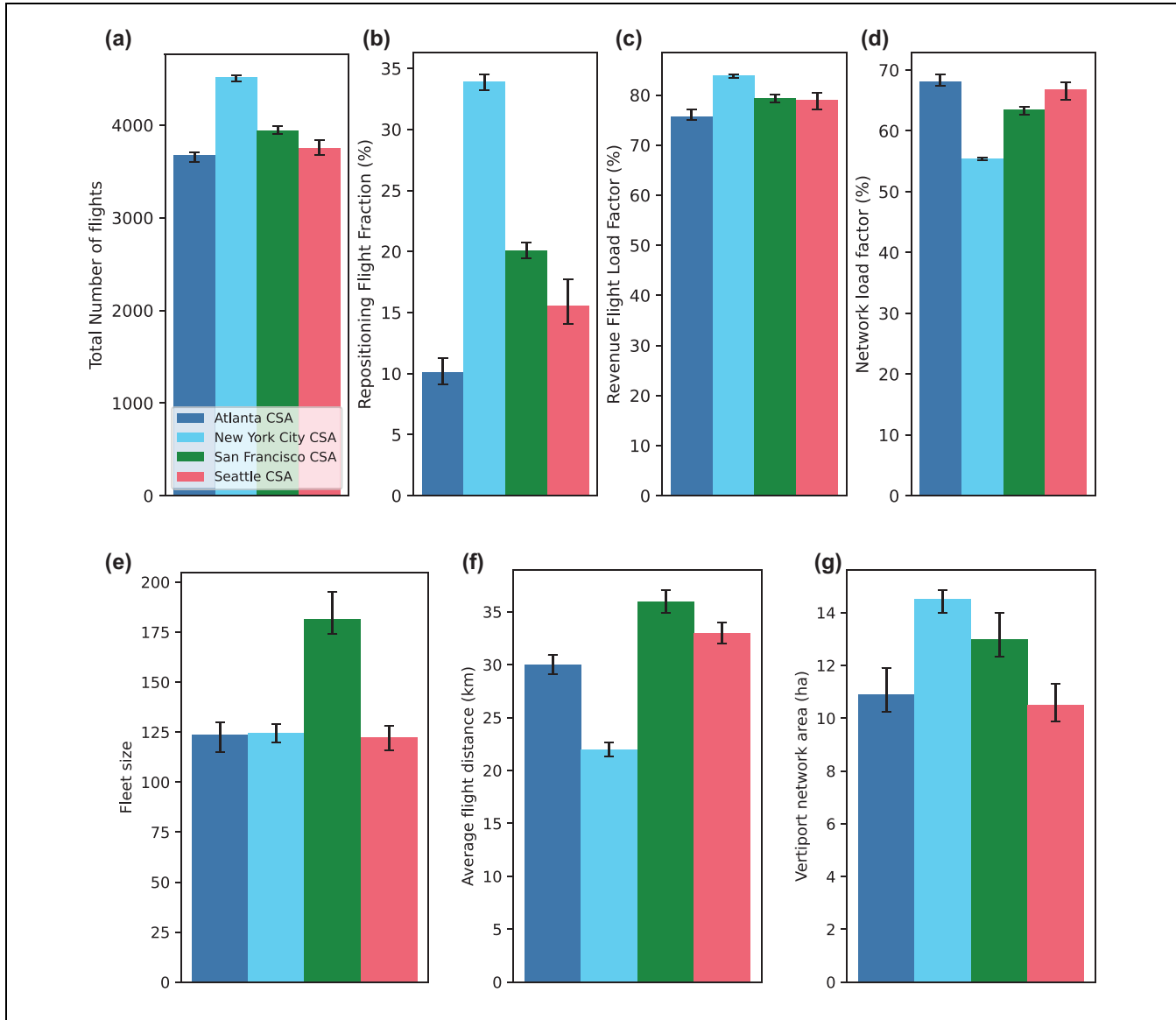


Figure 9. Sensitivity of number of flights, load factor, fleet size, average flight distance, and vertiport network area to city topology for the Atlanta, New York City, San Francisco, and Seattle combined statistical areas (CSAs) using a normalized daily volume of 10,000 passengers: (a) number of flights, (b) deadhead fraction, (c) revenue load factor, (d) network load factor, (e) fleet size, (f) average flight distance, and (g) vertiport network area.

for the Atlanta CSA using the rolling window scheduling formulation.

Passenger Demand. Results showing the sensitivity of scheduling and vertiport sizing results to demand, and specifically the sensitivity of fleet size, number of flights, load factor, vertiport network area, and vertiport composition to the daily passenger volume, are presented in Figure 10. Unsurprisingly, the fleet size and number of flights increase with higher passenger demand. Likewise, vertiport network area, along with the number of pads, gates, and parking spots, increases with higher passenger

demand because of the increased fleet size and the limited throughput of pads and gates. An increase is also observed in vehicle load factor because of an increased concentration of passengers available for aggregation, leading to a higher load factor on revenue flights. It should be noted that the presence of deadhead repositioning flights and the low volume of demand during off-peak commuting periods significantly reduces the overall load factor reported in Figure 10a. Load factor approaches 100% for revenue flights during peak commuting flow periods (10,000 passengers per day), as shown in Figure 6. Also note that the optimal number of flights in an the ideal situation where load factor is equal

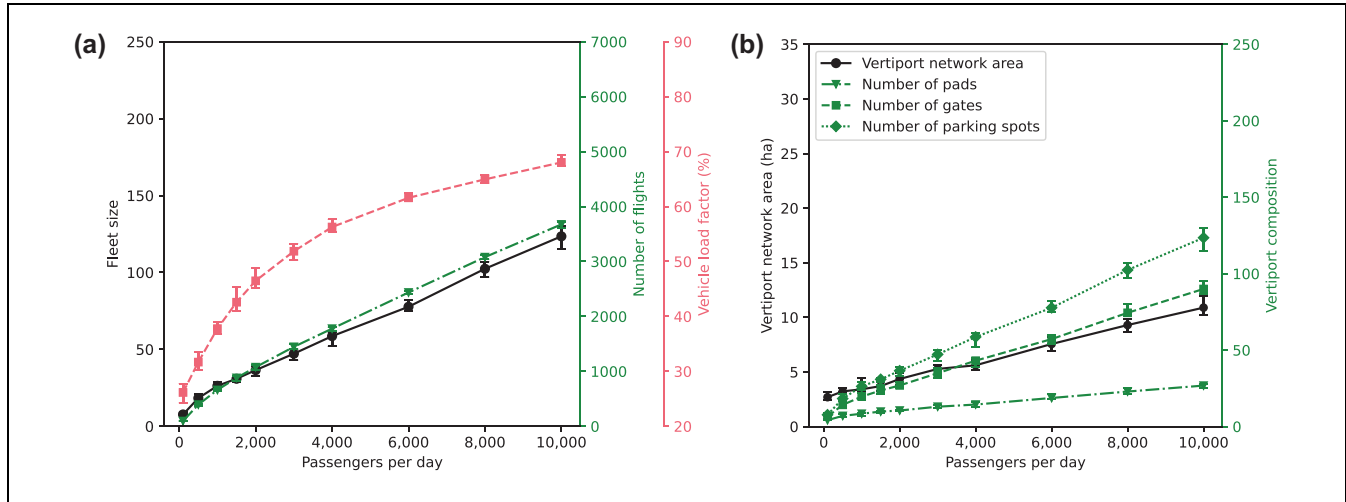


Figure 10. Sensitivity of (a) fleet size, number of flights, and vehicle load factor and (b) vertiport network area and vertiport composition to demand (number of passengers per day).

to 100% and no repositioning flights are needed is simply the daily passenger volume divided by the aircraft passenger capacity.

Passenger Aggregation Window. The impact of the passenger aggregation window on scheduling results is illustrated in Figure 11. We can observe that an increase in the passenger aggregation window tends to increase the vehicle load factor and reduce the number of required flights. This is a result of longer aggregation windows increasing the flexibility of the operator to aggregate a greater number of passengers before aircraft departure, thereby directly increasing the vehicle load factor. Furthermore, an increase in load factor reduces the number of revenue flights and leads to a reduction in the number of necessary repositioning flights.

A decrease in revenue and repositioning flights during peak flow conditions causes a corresponding decrease in fleet size and vertiport size, as illustrated in Figure 11, *a* and *b*, respectively. Increasing the passenger aggregation window in our commuting scenario yields diminishing returns because of the low impact of passenger aggregation window outside of peak hours, and the presence of deadhead repositioning flights, which cannot be eliminated because of demand flow imbalances. It should be noted, however, that the rolling schedule formulation does not fully benefit from the flexibility of a larger passenger aggregation window because it handles revenue flight assignment during preprocessing rather than being part of the optimization formulation.

Battery Charge Rate. Results illustrating the sensitivity of battery charge rate on scheduling and vertiport sizing

results are provided in Figure 12. A significant decrease in fleet size can be observed at higher battery charge rates because of the large fraction of the fleet that needs charging during peak flow conditions, as shown in Figure 6. At higher charge rates, the time required to recharge aircraft after each flight is reduced, allowing for quicker vehicle turnaround time and reducing the need to introduce additional aircraft into the fleet to meet demand. Although this leads to a corresponding decrease in the number of gates and parking spots required, the overall area requirement remains unchanged, since area is generally driven by number of pads (with the assumption that pad area and pad clearance area can be dynamically repurposed) which is not affected by charge rate. A slight increase in number of flights and an associated decrease in load factor can also be observed in Figure 12*a* because of an increase in repositioning flights that are necessary as a result of the smaller fleet size needing to fulfill the same number of revenue flights.

The sensitivity of scheduling and sizing results to vehicle speed is not presented but is anticipated to follow similar trends as those presented for battery charge rate, with the exception of gate area requirements, which will remain unchanged assuming that the power consumption per trip remains the same. Likewise, the sensitivity of scheduling and sizing results to an increase in aircraft power consumption is expected to have a similar but opposite trend compared with recharge rate because higher power consumption will lead to longer recharge times in a similar manner as a lower recharge rate.

Vehicle Passenger Capacity. Next, the sensitivity of scheduling and sizing results to vehicle passenger capacity, given

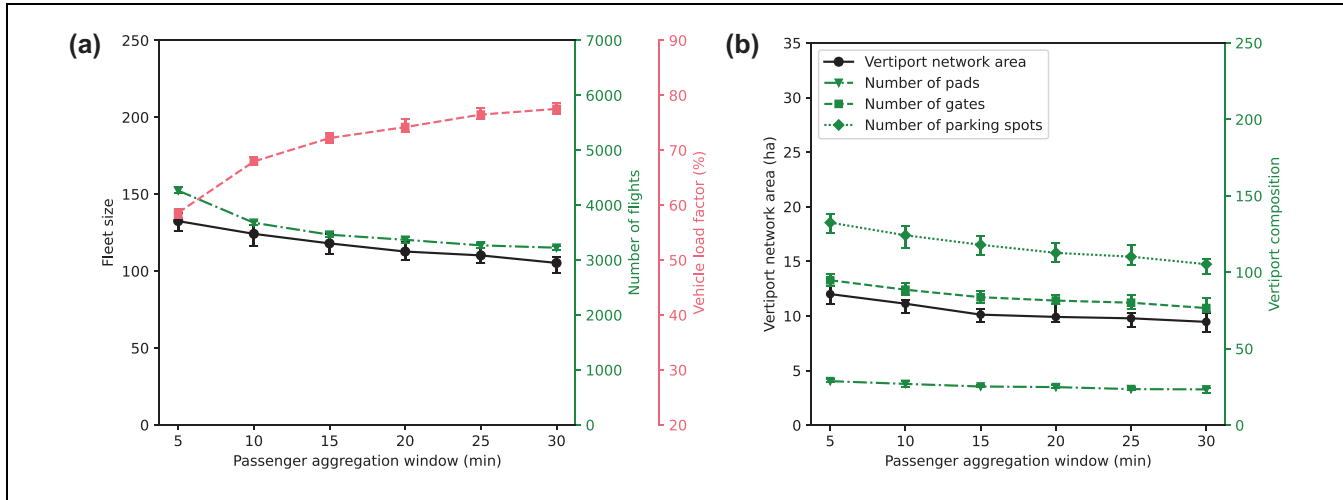


Figure 11. Sensitivity of (a) fleet size, number of flights, and vehicle load factor and (b) vertiport network area and vertiport composition to the passenger aggregation window size.

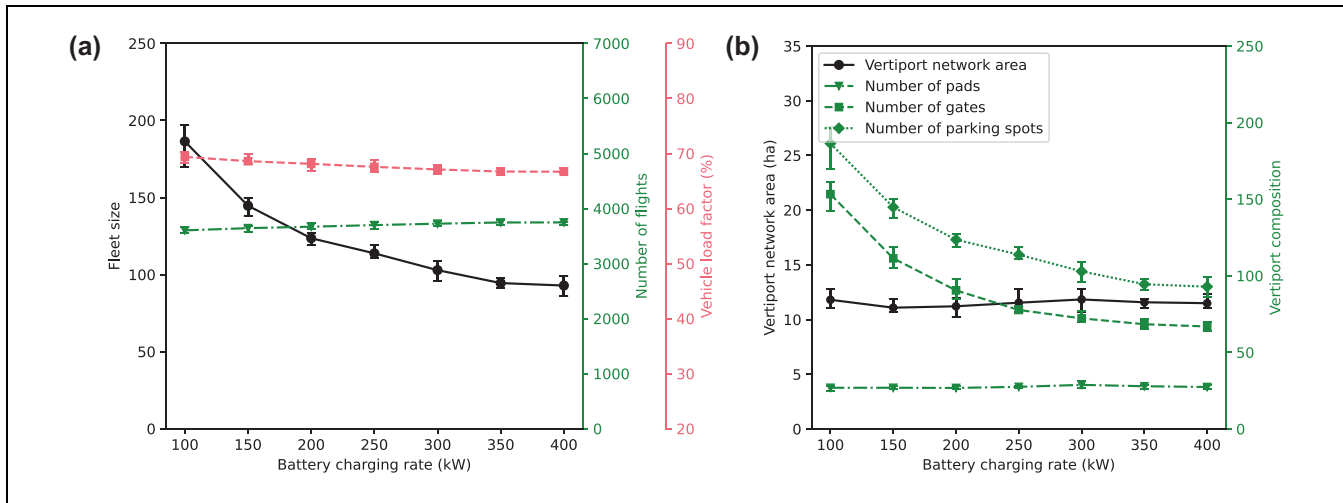


Figure 12. Sensitivity of (a) fleet size, number of flights, and vehicle load factor and (b) vertiport network area and vertiport composition to the battery charging rate.

in Figure 13, is explored. As can be expected, a significant reduction in fleet size and number of flights is possible with an increased vehicle seating capacity. Unlike results for battery charge rate, an increase in seating capacity directly reduces revenue flights during peak demand periods, which in turn decreases fleet size. A reduced number of revenue flights also leads to a decrease in repositioning flights, since there is a decrease in the amount of flow to balance. A reduction in the total number of flights during peak flow conditions also reduces the number of vertiports pads required, which leads to a reduced vertiport network area, as shown in Figure 13b. The reduced fleet size and number of flights also has the benefit of reducing the required number of gates and parking spots. Lastly, a significant decrease in overall vehicle load factor can be

observed in Figure 13a. This reduction is primarily because of a low load factor during off-peak flow conditions, where only one or two passengers are loaded onto each flight, and to the short passenger aggregation window of 10 min, which is not long enough to aggregate 8 passengers except during peak flow conditions.

Pad Clearance Time. The remainder of the sensitivity parameters considered (pad clearance time, vehicle dimension, FATO width, and FATO-FATO separation) have no impact on the implemented scheduling formulations and therefore have no impact on fleet sizing, number of flights, or vehicle load factor. Consequently, only vertiport sizing results are presented for these sensitivity parameters.

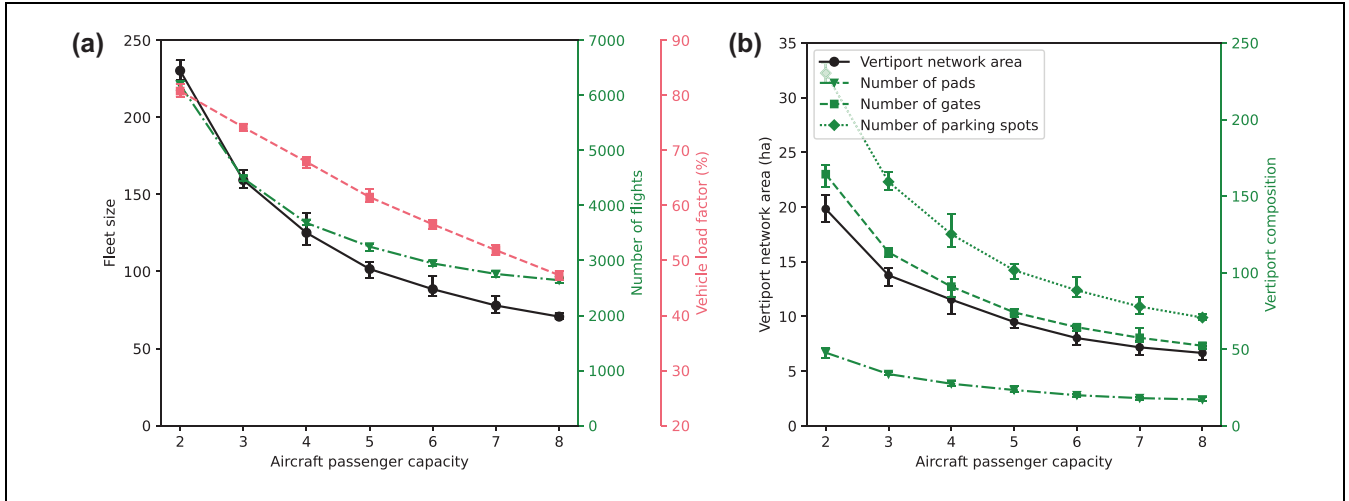


Figure 13. Sensitivity of (a) fleet size, number of flights, and vehicle load factor and (b) vertiport network area and vertiport composition to vehicle passenger capacity.

The sensitivity of vertiport area to pad clearance time is illustrated in Figure 14. Note that we define “pad clearance time” as the amount of time that a vertiport pad is dedicated to the approach or departure of a single vehicle and includes landing or takeoff time, as well as time required to taxi while in the vicinity of the pad. In other words, pad clearance time is the time that a pad is reserved for the arrival or departure of an aircraft, after which the pad is available for use by another aircraft or available to be repurposed as parking or gate area if necessary. It follows, therefore, that an increase in pad clearance time increases the number of pads required for a given flow of vehicles.

For pad clearance times below 60 s, however, the number of pads has dropped sufficiently such that the clearance area between pads no longer exceeds the area necessary for gate and parking infrastructure, leading to vertiport network area stabilizing even while the number of pads is decreasing. This can be expressed more explicitly if we consider the definitions for pad clearance area that assume a FATO–FATO separation of 61 m (200 ft), given in Equations 31 and 32. Assuming a vehicle size (D) of 15 m (50 ft), we can replace the separation distance by $4D$ to obtain:

$$A_{\text{clearance},q,t} = 3D(4D - D)(N_{\text{pads},q,t} - 1) \quad (33a)$$

$$= 9D^2(N_{\text{pads},q,t} - 1) \quad (33b)$$

meaning that the number of gates and parking spots need to be approximately equal or greater than nine times the number of pads required for a given time interval in order for them to fully utilize the available clearance area and affect the total vertiport area (assuming an area requirement of D^2 for gates and parking spots).

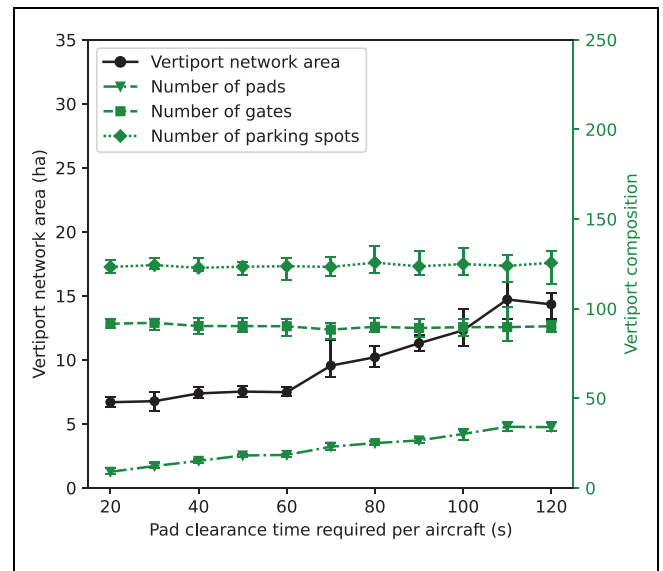


Figure 14. Sensitivity of vertiport network area and vertiport composition to pad clearance time.

This limit is reached in Figure 14 for pad clearance times below 60 s. The number of gates and parking spots is not affected. Note that changes to pad clearance time have no impact on scheduling results because pad clearance time does not affect passenger boarding time, recharge duration, or flight duration.

Vehicle Size. Vehicle dimension has a more straightforward effect on vertiport area, since it reduces the area requirements of parking and gate infrastructure in addition to pad infrastructure, and consequently has no

impact on vertiport composition, as shown in Figure 15. As can be observed, a reduction in the vehicle dimension used for vertiport infrastructure sizing from 50 ft (utilized by the FAA in Meyers and representative of the wingspan of the Archer Midnight eVTOL aircraft) to 35 ft (representative of the Joby S4 eVTOL aircraft) reduces vertiport area requirements by approximately 40% (9, 34, 35).

Pad Size. Finally, the impact of relaxing vertiport design safety margins is explored in Figures 16 and 17. First, considering changes to the width of the FATO area, we find a similar trend as those for vehicle dimension if the FATO width is above $1.5D$, since FATO width and vehicle dimension affect pad size in a similar manner, and because pad size drives vertiport area requirements for FATO widths in that range.

When the FATO width drops below $1.5D$, however, the pad clearance area gradually becomes saturated for several of the vertiports in the network, leading to further decreases in FATO width having a muted impact on vertiport area requirements. Revisiting Equation 33b, we can observe that following EASA guidelines for pad sizing (FATO width and safety area of $1.5D$ and $0.25D$, respectively) reduces pad clearance area to $4D^2(N_{pads, q, t} - 1)$, meaning that gates and parking infrastructure starts to saturate pad clearance area when there are approximately four times more gates and parking spots than number of pads. The reader is reminded that a linear relationship between safety area and FATO width is assumed such that a safety area of $0, 0.25 D, 0.5 D$ corresponds to a FATO

width of $1 D, 1.5 D,$ and $2 D,$ the latter two of which coincide with EASA and FAA guidance, as noted in Table 1.

Interestingly, a slight increase in the number of pads required can be observed for FATO widths below $1.5 D$ as a result of the optimizer prioritizing a reduction in parking requirements for vertiports where the clearance area has been saturated, since the number of pads no longer drives the area requirement for those vertiports. Using the baseline parameters defined in Table 2, the

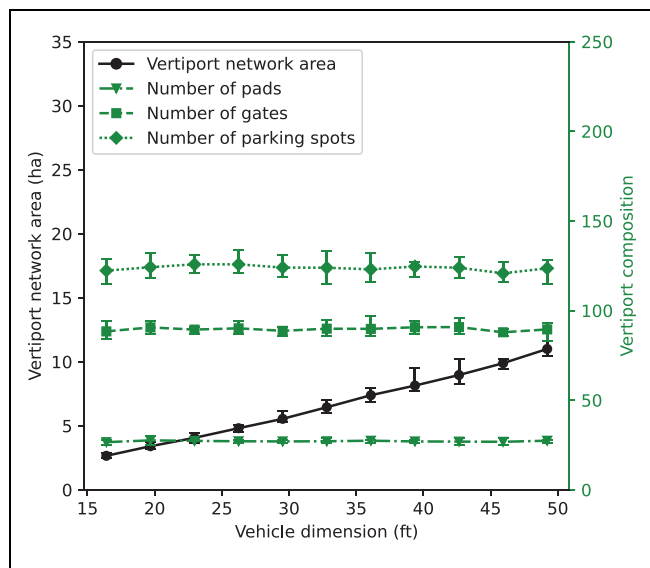


Figure 15. Sensitivity of vertiport network area and vertiport composition to urban air mobility vehicle size.

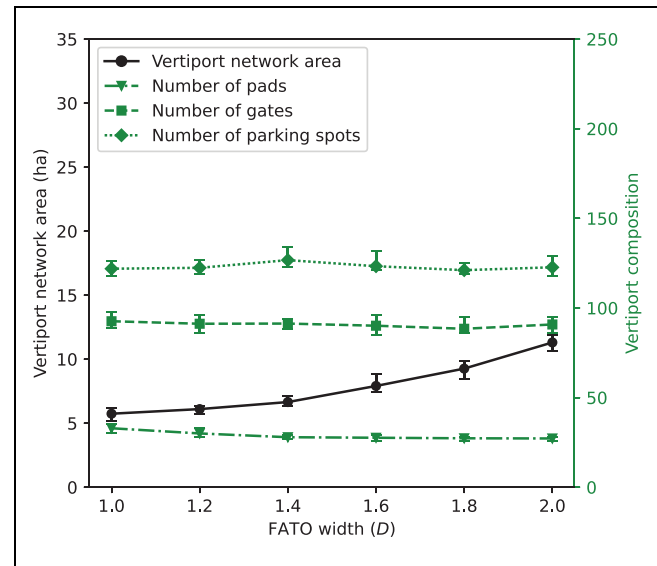


Figure 16. Sensitivity of vertiport network area and vertiport composition to final approach and take-off (FATO) width.

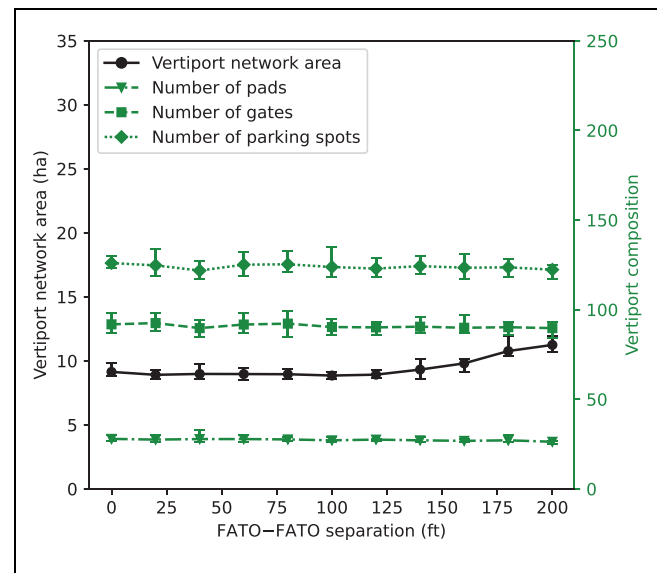


Figure 17. Sensitivity of vertiport network area and vertiport composition to final approach and take-off (FATO)-FATO separation.

required area for vertiport infrastructure can be reduced by approximately 40% (from 10.7 ha to 6.7 ha) by following EASA rather than FAA vertiport sizing guidelines.

Pad Separation. Likewise, vertiport area becomes dependent on parking area requirements because of the saturation of pad clearance area when reducing the separation necessary between pads for parallel approach and departure operations (reducing the distance between FATOs' area boundaries). Revisiting Equation 33b, we can observe that reducing the FATO–FATO separation from 61 m (200 ft) to 30 m (100 ft) decreases pad clearance area to $3D^2(N_{\text{pads},q,t} - 1)$, meaning that the number of gates and parking spots need only to be approximately equal or greater than three times the number of pads required for a given time interval in order for them to fully utilize the available clearance area and affect the total vertiport area, thereby greatly increasing the relevance of gate and parking area to overall vertiport area requirements. This behavior can be observed in Figure 17, where a decrease in FATO–FATO separation distance from 200 ft to 125 ft reduces the total vertiport area. No reduction in vertiport network area can be observed below this separation distance because any remaining clearance area is saturated with gate and parking area. It is important to highlight, however, that this behavior is a result of our assumptions that parking and gate infrastructure can utilize pad clearance area and that unused pad area can be used to park aircraft during off-peak periods.

Comparison with Approximate Formulations

Approximations of fleet size, number of flights, and vertiport area requirements obtained under ideal simplified conditions are provided below to enable rapid estimation of fleet and vertiport size, to help clarify the behavior of the sensitivity results, and to lend context to comparison of results with other published studies.

Number of Flights. First, considering the number of flights to meet a given daily passenger volume, it is clear that approximating number of flights is trivial if repositioning flights are ignored and passenger load factor is assumed to be constant, and is given by Equation 34:

$$N_{\text{flights}} \approx \frac{\sum_t \varphi_t}{n_{\text{pax}} \bar{L}_F} \quad (34)$$

where

N_{flights} = the number of flights necessary to transport a daily volume of $\sum_t \varphi_t$ passengers (where φ_t is passenger demand at time t) given that aircraft have a passenger capacity of n_{pax} and an average passenger load factor of \bar{L}_F .

Using this relation, we can estimate the number of flights to transport 10,000 passengers using aircraft with a four-passenger capacity and average load factor of 70%, to be 3,571 flights, which lines up well with results presented in Figure 10. Using a load factor of 100%, we can quickly find the minimum possible number of revenue flights necessary for a given daily passenger volume.

Fleet Size. Fleet size and vertiport area, on the other hand, depend on peak flow conditions rather than total daily demand. Assuming a constant flow of passengers over the peak flow period, fleet size can be approximated as the maximum outflow of vehicles over a single time step multiplied by the average number of time steps associated with vehicle block time and turnaround time (the number of time steps required to transport passengers, recharge the vehicle, and return it to the pool of available aircraft). In cases where vehicle flow is not constant, however, vehicle flow must also be averaged over this time period to obtain a reasonable approximation for fleet size. In this work, block time and turnaround time are given by the average flight duration, \bar{t}_{flight} , and average aircraft charge duration, which can be approximated from the ratio of aircraft power consumption to battery charge rate, $P_{\text{avg}}/B_{\text{charge}}$. Maximum average vehicle flow can then be approximated by averaging the maximum outflow of passengers, $\hat{\varphi}_t$, over this time period, and dividing by the aircraft passenger capacity and load factor. An estimate of fleet size is obtained by multiplying these terms together, as shown in Equation 35:

$$N_{\text{aircraft}} \approx \frac{\bar{\hat{\varphi}}_t}{n_{\text{pax}} \bar{L}_F} \left(\frac{P_{\text{avg}}}{B_{\text{charge}}} + 1 \right) \bar{t}_{\text{flight}} \quad (35)$$

Applying Equation 35 to our Atlanta vertiport network, which has an average trip duration of 6 min (corresponding to a 30 km leg with a speed of 300 km/h), a power consumption-to-recharge ratio of 1.5, a load factor of 80% (during peak flow conditions) and a four-passenger seating capacity, then the formulation simplifies to $N_{\text{aircraft}} \approx 4.7 \hat{\varphi}_t$. Considering a peak flow of 24.7 passengers per minute (corresponding to the flow of 740 passenger per half-hour given in Figure 3) we obtain a fleet size of 116 vehicles, which is lower than the fleet size of 121 obtained from our analysis for Atlanta shown in Figure 9e. The higher fleet size obtained in our analysis is a result of sampling the temporal demand distribution (Figure 3), which tends to bring peak flow concentrations closer to around 33 passengers per minute, which would bring the fleet size up to 155 vehicles if this flow rate was assumed to be constant over the peak flow period. Since passenger flow is not constant, maximum

passenger flow must be averaged, which results in the fleet size of 121 vehicles obtained earlier in the paper.

This result highlights the limitations of the rolling window scheduling approach, which, in its current implementation, only makes a limited attempt to flatten demand flow peaks during preprocessing, leading to less than optimal fleet sizes. This limitation can be resolved either by directly optimizing revenue flights in addition to repositioning flights, or by further preprocessing the demand schedule to be more uniform in nature (either by rescheduling revenue flights or by rejecting a portion of demand during peak flow conditions). This limitation has a more severe impact on vertiport sizing, since vertiport area is characterized by the maximum flow rate averaged over fewer time steps.

Vertiport Network Area. Since we assume that pad clearance area can be shared with gate and parking area and that taxiing route requirements can be ignored, vertiport area (for the baseline parameters in Table 2) is generally well approximated by the pad and clearance area, given by Equation 36:

$$A_{q,t} \approx N_{\text{pads},q,t} A'_{\text{pad}} + (N_{\text{pads},q,t} - 1) A'_{\text{clearance}} \quad (36)$$

Assuming a constant vehicle flow over a period of f_{pad}^{-1} (corresponding to one-and-a-half time steps for a pad clearance time, t_{pad} , of 90 s and a schedule time increment, Δt_s of 60 s), then we obtain,

$$A_{q,t} \approx \frac{f_{q=r,t}}{f_{\text{pad}}} (A'_{\text{pad}} + A'_{\text{clearance}}) - A'_{\text{clearance}} \quad (37)$$

where it should be noted that $f_{q=r,t}$ includes vehicles arriving and departing vertiport q at time t . Converting vehicle flow, $f_{q=r,t}$, to passenger departure flow, $\phi_{q,t}$, approximating incoming and outgoing vehicle flow to be approximately double of outgoing revenue vehicle flow during peak flow conditions, and using a vehicle size of 15 m (50 ft), along with a FATO width of $2D$, a safety area width of $0.5D$, and a FATO–FATO separation distance of 61 m (200 ft), we obtain:

$$A_{q,t} \approx \frac{36D^2 \hat{\phi}_{q,t}}{f_{\text{pad}} n_{\text{pax}} L_F} - 9D^2 \quad (38)$$

Using values of 15.24 m (50 ft) for vehicle size, 90 s for pad throughput, a load factor of 90%, a vehicle passenger capacity of four, generalizing terms to the vertiport network (composed of five vertiports) rather than a specific vertiport q , and recognizing that vertiport area is equal to the maximum area over time, Equation 38 becomes $A \approx 3484 \hat{\phi}_t - 5 \cdot 2090$. Substituting a peak passenger flow value of 33 passengers per minute identified for the Atlanta network, we obtain a network vertiport

area of 10.5 ha, which has good agreement with the 10.7 ha identified in Table 3.

Vertiport Network Area Throughput. To facilitate comparisons with other published studies, it is also useful to define the vertiport area required per passenger per hour, referred to as “vertiport area throughput, \dot{A} ,” in this work. We can approximate this metric in two ways. First, given that a time increment of 1 min is used in the scheduling formulation, and that the number of passengers that a pad can process per hour (including arrival and departure) can be approximated by $30f_{\text{pad}} n_{\text{pax}} L_F$, we can define the vertiport network area (for a five vertiport network) required to accommodate a throughput of one passenger per hour as:

$$\begin{aligned} \dot{A} &\approx \frac{A'_{\text{pad}} + A'_{\text{clearance}} - 5A'_{\text{clearance}} N_{\text{pads}}^{-1}}{30f_{\text{pads}} n_{\text{pax}} L_F} \\ &\approx \frac{D^2}{72} (18 - 45N_{\text{pads}}^{-1}) \\ &\approx 58.1 - 145.1N_{\text{pads}}^{-1} \end{aligned} \quad (39)$$

Equivalently, dividing Equation 38 by departing passenger flow per hour and generalizing the result to the vertiport network:

$$\begin{aligned} \dot{A} &\approx \frac{36D^2}{60f_{\text{pad}} n_{\text{pax}} L_F} - \frac{45D^2}{60\hat{\phi}_t} \\ &\approx 58.1 - 174.2\hat{\phi}_t^{-1} \end{aligned} \quad (40)$$

which reduces to an area throughput of approximately 52.8 m^2 per passenger per hour. Note that this area includes the vertiport area required at both the arrival and departure vertiport and that it is sensitive to pad topology, vehicle dimension, pad throughput, load factor, and vehicle passenger capacity.

Equations 39 and 40 approximate the area throughput under the assumption that vehicle or passenger flow is constant, which ignores the bimodal nature of commuting demand. We can also directly approximate area throughput from earlier scheduling and vertiport sizing results. For example, if we consider that a vertiport network size of 10.7 ha is required to transport 1,450 passengers during the hour associated with peak flow conditions, then the vertiport network has an average area throughput of 73 m^2 per passenger per hour. Furthermore, if we consider a full day of operations with a total of 10,000 passengers over 24 h, then the vertiport network has an average area throughput of 257 m^2 per passenger per hour, which highlights the challenge of operating a UAM service with a highly nonuniform temporal demand distribution.

Given that flow nonuniformity increases fleet and infrastructure downtime and therefore decreases profitability, UAM operators will likely seek to mitigate sources of nonuniform flow, for example by aggregating demand from multiple sources with different temporal distributions, or by limiting the fraction of demand served during peak flow conditions. Consequently, vertiport area throughput values based on peak flow conditions are more meaningful for comparison with other studies and for future work in this research area. It should also be noted that the vertiport area sensitivity results described by Figures 14 to 17 also apply to area throughput. For example, area throughput (during peak flow) can be improved to 28.4m^2 per passenger per hour by following EASA pad sizing guidelines, and further improved to 23.5 and 21.1m^2 per passenger per hour if we reduce FATO–FATO separation to 38 m (125 ft) and also increase load factor from 90% to 100%. Further reduction in pad sizing or pad separation, however, leads to pad clearance area saturation, at which point gate and parking area need to be considered. Likewise, gate and parking area need to be considered if we remove the assumption that parking and gate infrastructure can utilize pad clearance area, or if we no longer assume that unused pad area can be used to park aircraft.

Comparison with Previous Studies

Several published studies have examined how operational parameters affect vertiport sizing for UAM operations. While it is challenging to compare our results directly with those of other studies because of differences in demand-flow data, scheduling approach, and vertiport sizing methodology, the comparison nonetheless demonstrates the advantages, limitations, and differences of the methods implemented in our work, and offer useful insights for further research in this field.

Vascik and Hansman developed an integer programming approach to determine the sensitivity of vertiport capacity to vertiport topology parameters, such as number of gates and pads, and to operational parameters, such as vehicle turnaround time and taxi time (5). A linear topology similar to the one proposed in our work is considered, but differences in vertiport sizing parameters significantly reduce area requirements. Most notably: 1) a vehicle dimension, D , of 45 ft is used rather than 50 ft, 2) EASA guidelines for pad sizing are followed rather than FAA guidelines, and 3) a pad separation of approximately 200 ft is enforced between FATO area centerlines rather than FATO area edges. Consequently, Vascik and Hansman find that an area of $1,505\text{m}^2$ is required for each independent vertiport pad in a linear configuration beyond two, compared with $4,180\text{m}^2$ and $2,555\text{m}^2$ found

in our work, following FAA and EASA vertiport guidelines, respectively (5).

Zelinski presented several generic vertiport topology designs and evaluated their relative surface area utilization and operational efficiency (11). Zelinski also used a vehicle dimension of 45 ft and followed EASA pad sizing guidelines but enforced a minimum FATO–FATO edge separation of 200 ft. Several four-pad vertiport designs are presented in Zelinski ranging from $3,809\text{m}^2$ to $5,760\text{m}^2$ per pad (11). It should be noted, however, that the vertiport topologies considered by Zelinski include considerations for taxiways and connectivity between pads and parking spaces. As a result, area requirements per pad are higher than those found in our work, which is expected given that our vertiport topology aims to identify a lower bound on vertiport area requirements.

Taylor et al. used a stochastic Monte Carlo simulation to calculate vehicle throughput for several vertiport configurations and found that 420m^2 is needed to accommodate an additional vehicle per hour (12). In their study, a vehicle size of 50 ft was used and FAA pad sizing guidelines were followed but the enforced pad clearance time is unclear. In comparison, we found that only 190m^2 is needed to accommodate an additional vehicle per hour for a vertiport already containing several pads (a lower area is required per vehicle for a vertiport with a single pad since it has no clearance area requirements).

Preis et al. have published several studies related to vertiport design and sizing, including one where four vertiport topologies were introduced and a mixed integer programming approach was implemented to find the topology and number of pads and gates that maximizes vertiport throughput (14). The study demonstrated the sensitive nature of vertiport throughput, with values ranging from 26 to 56m^2 per passenger per hour (assuming pilotless operation) for vertiports sized to fit within specific areas near train stations in three cities in Germany. Sizing was also performed for several vertiport topologies following EASA pad sizing guidelines, using a FATO–FATO separation of 61 m (200 ft), and using a pad clearance time of 60 s for several vehicle sizes. Area throughput requirements for a vehicle with a tip-to-tip span of 15.7 m (51.5 ft), using a pad clearance time of 60 s, were found to range between 14 and 25m^2 per passenger per hour assuming a vehicle passenger capacity of 15. Adjusting these area requirements for a similarly sized vehicle with a passenger capacity of only four using Equation 39 gives us a vertiport throughput range of 52 to 93m^2 per passenger per hour. Likewise, adjusting area requirements to correspond to the pad clearance time of 90 s used in our work increases the area to 79 to 105m^2 per passenger per hour. These results illustrate the strong sensitivity of vertiport sizing to vehicle and operational parameters and highlight the importance for city

planners, policymakers, and operators to understand the sensitivity of vertiport size to these parameters.

Conclusions

A scalable fleet scheduling formulation was presented in this paper that is capable of minimizing both fleet size and repositioning deadhead flights. Additionally, an implementation of vertiport network area as a secondary objective to the scheduling formulations was provided. The presented scheduling formulations are linear, well approximated by a continuous formulation, and single-commodity, allowing them to scale to problem sizes representative of a full day of UAM operations. A vertiport topology and sizing methodology was also presented that aims to facilitate identification of a lower bound on vertiport area requirements and to clarify the sensitivity of area requirements to aircraft and operational parameters. The presented topology and results provide a lower bound area estimate for a given set of aircraft and operational parameters by: 1) ignoring the aspect ratio of the vertiport footprint, 2) ignoring taxiing area and associated gate–pad or gate–parking connectivity, 3) using a topology with simultaneous independent operations in mind, 4) allowing gate and parking infrastructure to make use of pad clearance area, and 5) allowing pad area to be repurposed to parking area during off-peak periods.

Scheduling results and vertiport sizing results were provided and compared for a five-vertiport network for Atlanta, New York City, Seattle, and San Francisco, with vertiport locations based on previous work described in Kotwicz HERNICZEK and German (24). We find that the temporal flow distribution, flow imbalance, and average flight distance notably affect fleet sizing and vertiport sizing for a given daily passenger volume. An increase in average flight distance was found to have a similar effect as reducing flight speed or reducing battery recharge rate and effectively increases the fleet size necessary to meet passenger demand. An increase in flow imbalance increases the number of repositioning flights necessary, primarily increasing total number of flights but also slightly increasing fleet size. Lastly, an increase in the temporal flow distribution concentration, that is, increasing the maximum flow of passengers for a given time interval, directly increases both fleet size and vertiport network area, since both must be sized to handle peak flow conditions.

The sensitivity of scheduling and vertiport sizing results (specifically the sensitivity of fleet size, number of flights, passenger load factor, vertiport network area, and vertiport composition) to several aircraft and operational parameters is explored, including sensitivity to daily passenger volume, battery recharge rate, aircraft

passenger capacity, vehicle size, vertiport pad clearance time, pad size, and pad separation. Unsurprisingly, daily passenger volume and aircraft passenger capacity each have a significant impact on fleet size and vertiport network area. Battery recharge time was found to have a significant impact on fleet size because of the recharge rate being comparable with aircraft power consumption, which causes a significant fraction of the fleet to require charging during peak flow conditions. Likewise, pad clearance time, vehicle dimension, FATO width, and FATO–FATO separation were all found to greatly affect vertiport network area. Notably, we found that vertiport area was largely independent of the number of required parking spots and gates because the required clearance area between pads for simultaneous independent operations was sufficient to accommodate gate and parking infrastructure. In special cases, however, we found that vertiport area became dependent on parking area requirements rather than pad area because of the pad clearance area becoming saturated. In this work, we observed this to occur when pad clearance time dropped below 60 s, when FATO–FATO separation decreased below 125 ft, and when the FATO width was less than 1.5D.

Approximate formulations were also developed for fleet and vertiport sizing requirements that clarify their sensitivity to vehicle and operational parameters and facilitate comparison of results with previously published studies. We found that, even though the vertiport sizing methods in many of the referenced published studies shared similarities to our work, significant differences in sizing estimates were observed because of the sensitivity of vertiport area requirements to vehicle and operational parameters, highlighting the relevance of the sensitivity studies presented in our work and demonstrating a need for clearer guidelines on vertiport pad sizing, pad separation, vehicle sizing, and pad clearance time.

Based on the findings from the sensitivity studies and region-based results, several conclusions can be made. These include:

- 1) Using the vertiport topology and operational parameters described in the paper, vertiport sizing requirements drop approximately 40% when following EASA pad sizing guidelines rather than FAA vertiport guidelines.
- 2) Although a significant reduction in area is possible by adopting EASA guidance on pad sizing, by relaxing pad separation requirements for simultaneous independent operations, or by increasing pad throughput, the decrease in area may not be sufficient to enable centralized vertiport operations in dense urban areas, such as the Atlanta Downtown core, Seattle Central Business District, San Francisco Financial District, or Central

Manhattan. If a significant reduction in vertiport area requirements is not possible, scaled UAM operations in dense urban areas may be more feasible if commuting operations bring passengers from the suburbs to a less-densely-populated metro hub rather than directly to the downtown core. Likewise, use of several smaller nearby vertiports in urban areas rather a single large vertiport or use of vertically distributed vertiports may facilitate integration of vertiports onto existing structures and smaller parcels of land.

- 3) UAM operations are not well suited to commuting operations from the perspective of fleet sizing and vertiport network area because of the imbalanced and bimodal nature of commuting demand. Although the fleet size necessary to transport 10,000 passenger per day was found to be reasonable, the majority of the fleet and vertiport area is unused during off-peak periods because fleet size and vertiport area are determined by peak flow conditions. Additionally, the imbalanced nature of commuting flow leads to a large number of necessary repositioning flights which further increase operational costs. As a result, we anticipate scaled commuting operations to be generally unprofitable without a significant increase in vehicle passenger density or improvement in pad vehicle throughput. Furthermore, focusing on commuting operations that replace helicopter, float plane, or ferry operations, or focusing on operations with more stable demand, such as an airport air taxi mission, may also be more practical in the near term.

Although the present formulations contain several limitations, they enable scheduling and sizing of large vertiport networks and facilitate exploration of fleet and vertiport size sensitivity to vehicle and operational parameters. Furthermore, the implemented formulations and presented sensitivity studies provide insight into and may help inform vehicle design, vertiport configuration, and fleet management policy decisions.

Author Contributions

The authors confirm contribution to the paper as follows: study conception and design: Mark Kotwicz Herniczek, Brian German; data collection: Mark Kotwicz; analysis and interpretation of results: Mark Kotwicz; draft manuscript preparation: Mark Kotwicz. All authors reviewed the results and approved the final version of the manuscript.

Declaration of Conflicting Interests


The author(s) declared no potential conflicts of interest with respect to the research, authorship, and/or publication of this article.


Funding

The author(s) disclosed receipt of the following financial support for the research, authorship, and/or publication of this article: This work was supported in part by the National Aeronautics and Space Administration through cooperative agreement 80NSSC21M0113: Innovative Manufacturing, Operation, and Certification of Advanced Structures for Civil Vertical Lift Vehicles (IMOCAS).

ORCID iDs

Mark T. Kotwicz Herniczek  <https://orcid.org/0000-0002-1694-4853>

Brian J. German  <https://orcid.org/0000-0003-4448-0029>

Lukas Preis  <https://orcid.org/0000-0002-2610-7661>

References

1. Schweiger, K., and L. Preis. Urban Air Mobility: Systematic Review of Scientific Publications and Regulations for Vertiport Design and Operations. *Drones*, Vol. 6, No. 7, 2022, p. 179. <https://doi.org/10.3390/drones6070179>; <https://www.mdpi.com/2504-446X/6/7/179>.
2. Cheyno, E. Vertiport Design and Operations. *Proc., 4th Annual Meeting and Technical Display*, Anaheim, CA, American Institute of Aeronautics and Astronautics, October 23–27, 1967. <https://doi.org/10.2514/6.1967-891>; <https://arc.aiaa.org/doi/10.2514/6.1967-891>.
3. Holden, J., and N. Goel. Fast-Forwarding to a Future of On-Demand Urban Air Transportation. Technical Report. *Uber*, 2016. https://evtol.news/__media/PDFs/UberElevateWhitePaperOct2016.pdf
4. Vascik, P. D., and R. J. Hansman. Scaling Constraints for Urban Air Mobility Operations: Air Traffic Control, Ground Infrastructure, and Noise. *Proc., 2018 Aviation Technology, Integration, and Operations Conference, AIAA AVIATION Forum*, Atlanta, GA, American Institute of Aeronautics and Astronautics, 2018. <https://doi.org/10.2514/6.2018-3849>; <https://arc.aiaa.org/doi/10.2514/6.2018-3849>.
5. Vascik, P. D., and R. J. Hansman. Development of Vertiport Capacity Envelopes and Analysis of Their Sensitivity to Topological and Operational Factors. *Proc., AIAA SciTech 2019 Forum*, San Diego, CA, American Institute of Aeronautics and Astronautics, 2019. <https://doi.org/10.2514/6.2019-0526>; <https://arc.aiaa.org/doi/10.2514/6.2019-0526>.
6. Rimjha, M., and A. Trani. Urban Air Mobility: Factors Affecting Vertiport Capacity. *Proc., 2021 Integrated Communications Navigation and Surveillance Conference (ICNS)*, Dulles, VA, IEEE, New York, 2021, pp. 1–14. <https://doi.org/10.1109/ICNS52807.2021.9441631>.
7. Preis, L., and M. Hornung. Vertiport Operations Modeling, Agent-Based Simulation and Parameter Value Specification. *Electronics*, Vol. 11, No. 7, 2022, p. 1071. <https://doi.org/10.3390/electronics11071071>; <https://www.mdpi.com/2079-9292/11/7/1071>.
8. Brunelli, M., C. C. Ditta, and M. N. Postorino. New Infrastructures for Urban Air Mobility Systems: A Systematic

- Review on Vertiport Location and Capacity. *Journal of Air Transport Management*, Vol. 112, 2023, p. 102460. <https://doi.org/10.1016/j.jairtraman.2023.102460>. <https://www.sciencedirect.com/science/article/pii/S0969699723001035>.
9. Meyers, M. *Vertiport Design*. Memorandum EB 105, Federal Aviation Administration, 2022. <https://www.faa.gov/sites/faa.gov/files/eb-105-vertiports.pdf>
 10. EASA. Vertiports Prototype Technical Specifications for the Design of VFR Vertiports for Operation with Manned VTOL-Capable Aircraft Certified in the Enhanced Category. Technical Report. PTS-VPT-DSN. European Aviation Safety Agency, 2022. <https://www.easa.europa.eu/downloads/136259/en>.
 11. Zelinski, S. Operational Analysis of Vertiport Surface Topology. *Proc., 2020 AIAA/IEEE 39th Digital Avionics Systems Conference (DASC)*, San Antonio, TX, IEEE, New York, 2020, pp. 1–10. <https://doi.org/10.1109/DASC50938.2020.9256794>.
 12. Taylor, M., A. Saldanli, and A. Park. Design of a Vertiport Design Tool. *Proc., 2020 Integrated Communications Navigation and Surveillance Conference (ICNS)*, Herndon, VA, IEEE, New York, 2020. <https://doi.org/10.1109/ICNS50378.2020.9222989>.
 13. Guerreiro, N. M., G. E. Hagen, J. M. Maddalon, and R. W. Butler. Capacity and Throughput of Urban Air Mobility Vertiports with a First-Come, First-Served Vertiport Scheduling Algorithm. *Proc., AIAA AVIATION 2020 Forum*, American Institute of Aeronautics and Astronautics, June 15–19, 2020. <https://doi.org/10.2514/6.2020-2903>; <https://arc.aiaa.org/doi/abs/10.2514/6.2020-2903>.
 14. Preis, L. Quick Sizing, Throughput Estimating and Layout Planning for VTOL Aerodromes – A Methodology for Vertiport Design. *Proc., AIAA AVIATION 2021 Forum*, American Institute of Aeronautics and Astronautics, August 2–6, 2021. <https://doi.org/10.2514/6.2021-2372>; <https://arc.aiaa.org/doi/10.2514/6.2021-2372>.
 15. Goodrich, K. H., and B. Barmore. Exploratory Analysis of the Airspace Throughput and Sensitivities of an Urban Air Mobility System. *Proc., 2018 Aviation Technology, Integration, and Operations Conference*, Atlanta, GA, American Institute of Aeronautics and Astronautics, June 25–29, 2018. <https://doi.org/10.2514/6.2018-3364>; <https://arc.aiaa.org/doi/10.2514/6.2018-3364>.
 16. Li, S., M. Egorov, and M. J. Kochenderfer. Analysis of Fleet Management and Infrastructure Constraints in On-Demand Urban Air Mobility Operations. *Proc., AIAA AVIATION 2020 Forum*, American Institute of Aeronautics and Astronautics, June 15–19, 2020. <https://doi.org/10.2514/6.2020-2907>; <https://arc.aiaa.org/doi/10.2514/6.2020-2907>.
 17. Schweiger, K., F. Knabe, and B. Korn. UAM Vertidrome Airside Operation: What Needs to Be Considered? *Proc., Delft International Conference on Urban Air-Mobility (DICUAM)*, Braunschweig, 2021.
 18. Ploetner, K. O., C. Al Haddad, C. Antoniou, F. Frank, M. Fu, S. Kabel, C. Llorca, et al. Long-Term Application Potential of Urban Air Mobility Complementing Public Transport: An Upper Bavaria Example. *CEAS Aeronautical Journal*, Vol. 11, No. 4, 2020, pp. 991–1007. <https://doi.org/10.1007/s13272-020-00468-5>.
 19. Preis, L., and M. H. Vazquez. Vertiport Throughput Capacity Under Constraints Caused by Vehicle Design, Regulations and Operations. *Proc., Delft International Conference on Urban Air-Mobility*, Online, 2022, p. 12. <https://cdn.aanmelderusercontent.nl/i/doc/8fa60b7fc-fa71ea900ce2bea2037a151?forcedownload=True>.
 20. Mayor, T., and J. Anderson. Getting Mobility off the Ground. Technical Report. *KPMG*, 2019. <https://assets.kpmg.com/content/dam/kpmg/ie/pdf/2019/10/ie-urban-air-mobility.pdf>
 21. NEXA Advisors. Urban Air Mobility -Economics and Global Markets. Technical Report. *NEXA*, 2018.
 22. Goyal, R., C. Reiche, C. Fernando, J. Serrao, S. Kimmel, A. Cohen, and S. Shaheen. Urban Air Mobility (UAM) Market Study. Technical Report. HQ-E-DAA-TN65181. *NASA*, 2018. <https://ntrs.nasa.gov/citations/20190001472>.
 23. Kotwicz Herniczek, M. T., and B. J. German. Nationwide Demand Modeling for an Urban Air Mobility Commuting Mission. *Journal of Air Transportation*, 2023. <https://doi.org/10.2514/1.D0371>.
 24. Kotwicz Herniczek, M. T., and B. J. German. Vertiport Placement Optimization Methods for an Urban Air Mobility Commuting Service. *Transportation Research Record*, 2023, p.
 25. U.S. Census Bureau. *Census Data API: Time of Departure to Go to Work*. 2019. <https://api.census.gov/data/2019/acs/acs5/groups/B08302.html>.
 26. U.S. Census Bureau. *Census Data API: Mean Usual Hours Worked in the Past 12 Months*. 2019. <https://api.census.gov/data/2019/acs/acs5/groups/B23020.html>.
 27. Kotwicz Herniczek, M. T. *A Framework for the Analysis of an Urban Air Mobility Commuting Service*. PhD thesis. Georgia Institute of Technology, Atlanta, GA, 2023.
 28. Dermody, J. *Advisory Circular: Heliport Design*. Technical Report. 150/5390-2D. Federal Aviation Administration, 2023. https://www.faa.gov/documentLibrary/media/Advisory_Circular/AC_150_5390_2D_Heliports.pdf.
 29. Federal Aviation Administration. Industry Response to FAA Vertiport EB 105. Online, 2022.
 30. Justin, C. Y., A. P. Payan, S. I. Briceno, B. J. German, and D. N. Mavris. Power Optimized Battery Swap and Recharge Strategies for Electric Aircraft Operations. *Transportation Research Part C: Emerging Technologies*, Vol. 115, 2020, p. 102605. <https://doi.org/10.1016/j.trc.2020.02.027>.
 31. Brown, A., and W. L. Harris. Vehicle Design and Optimization Model for Urban Air Mobility. *Journal of Aircraft*, Vol. 57, No. 6, 2020, pp. 1003–1013. <https://doi.org/10.2514/1.C035756>; <https://arc.aiaa.org/doi/10.2514/1.C035756>.
 32. Duffy, M. J., S. R. Wakayama, and R. Hupp. A Study in Reducing the Cost of Vertical Flight with Electric Propulsion. *Proc., 17th AIAA Aviation Technology, Integration, and Operations Conference*, Denver, CO, American Institute of Aeronautics and Astronautics, 2017. <https://doi.org/>

- 10.2514/6.2017-3442; <https://arc.aiaa.org/doi/10.2514/6.2017-3442>.
33. Wassiliadis, N., J. Schneider, A. Frank, L. Wildfeuer, X. Lin, A. Jossen, and M. Lienkamp. Review of Fast Charging Strategies for Lithium-Ion Battery Systems and Their Applicability for Battery Electric Vehicles. *Journal of Energy Storage*, Vol. 44, 2021, p. 103306. <https://doi.org/10.1016/j.est.2021.103306>.
 34. Reim, G. Archer Unveils Midnight Production Vehicle. *Aviation Week Network*, 2022. <https://aviationweek.com/aerospace/advanced-air-mobility/archer-unveils-midnight-production-vehicle>.
 35. Vertical Flight Society. Joby Aviation S4. 2022. <https://evtol.news/joby-s4>.